CHAPTER-4

RESULTS AND DISCUSSION

Data collected were analysed to get bubble size distribution, Sauter-mean bubble diameter and specific interfacial area of bubbles from acoustic signals are presented in this chapter. The effect of static bed height, superficial gas velocity and vertical position in the column were studied on these properties were studied. The effect of physical properties of the liquid was studied by comparing results for all the four systems (distilled water, aq. Soln of NaOH, EG and CMC). Volumetric mass transfer coefficient in air-water ware estimated from the data obtained from mass-transfer studies.

4.1 Single Bubble studies:

Single bubble studies were carried out to understand the distance upto which condenser mike can capture the acoustic signals. Video recording were also made at a frame rate of 120 fps (frame per second).

4.1.1 Visual Observation:

A typical successive frames (equivalent to a gap of 0.00833 s) is shown in Figure 4,1(a) and (b). Most of the time, at least two bubbles were discharged from the nozzle. The bubbles velocity can be measured from successive frame. A close examination revealed that the bubbles are not moving vertically. The path deviates more from vertical path when a sequence of bubbles (continuous bubbling) was released from the nozzle (Figure 4.2).

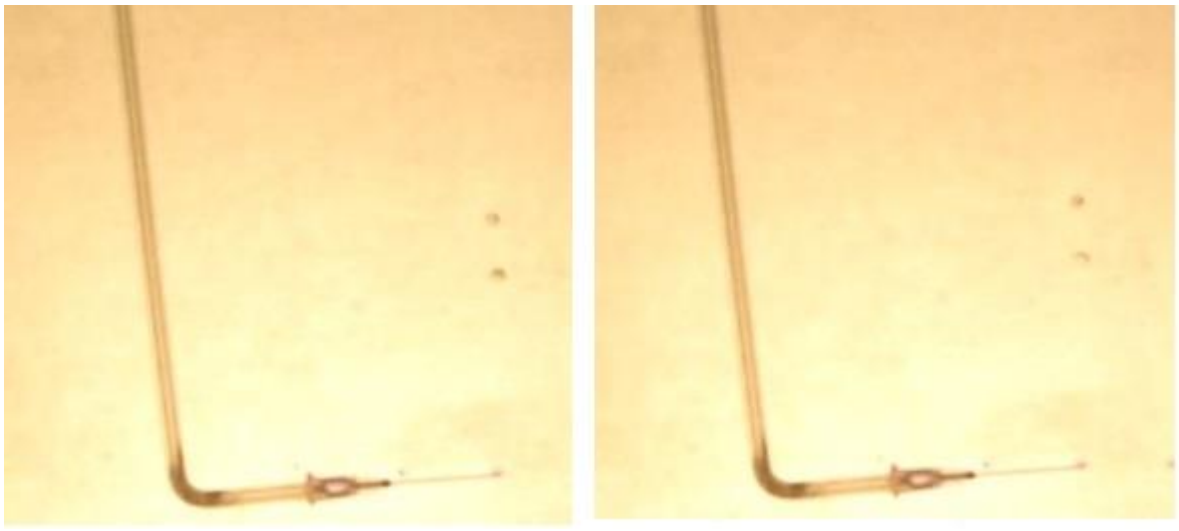

(a) (b)

Figure 4.1(a): A couple of bubbles moving up (b) Position of bubbles after a lapse of 0.00833 s.

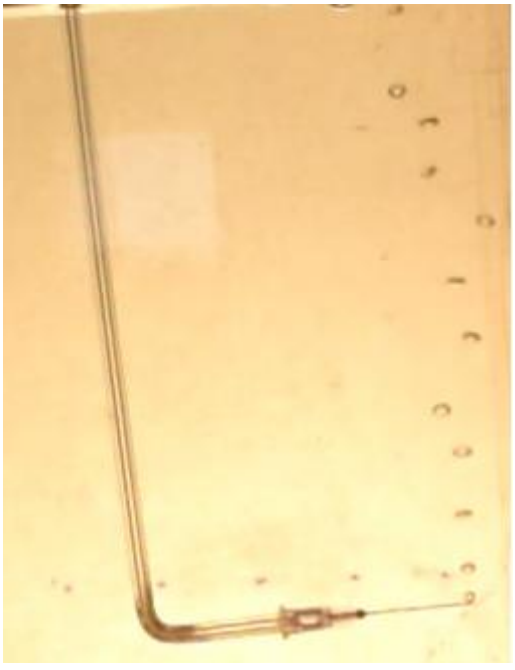

Figure 4.2: Bubbles do not move vertically during continuous bubbling.

Vertical velocity component can be computed from successive frames. The time interval between two successive frames were 1/120 = 0.00833 s. The distance travelled by a single bubble was 0.115 m. Since the bubble reached the upper surface of the liquid in 93 frames, the velocity of the bubble was =0.115/(93/120)= 0.148 m s^{-1}. The distance travelled by a bubble in successive frame is 0.115/93=0.00124 m.

4.1.2 Acoustic measurements:

Amplitude of a typical acoustic signal is presented in the Figure 4.3. The nozzle tip was positioned. The acoustic signal was normalized since the maximum value was 1. This signal shows data points and corresponding to approximately 0.5 s. It is due to a compound effect of low and high frequency signals. To further analyse the signal, Fast Fourier Transform, using MATLAB's "fft" function, was determined.

Acoustic signal for a short duration was chosen and a typical segment of about 0.01 s is shown in Figure 4.4. This segment has only two low frequency signal which died down quickly. The fast Fourier transform of this signal segment is shown in Figure 4.5 A prominent frequency occurs at 513 corresponding to the bubble diameter of 0.0062 m which is just above the nozzle internal diameter of 0.0056 mm. The distance from the wall was 0.01 m indicating that the mike is able to capture acoustic signals upto a distance of 0.01 m in its close proximity.

While studying the bubble behaviour in bubble columns the contribution to several other bubbles make the volume pulsation frequencies more prominent than the low frequencies due to other phenomena.

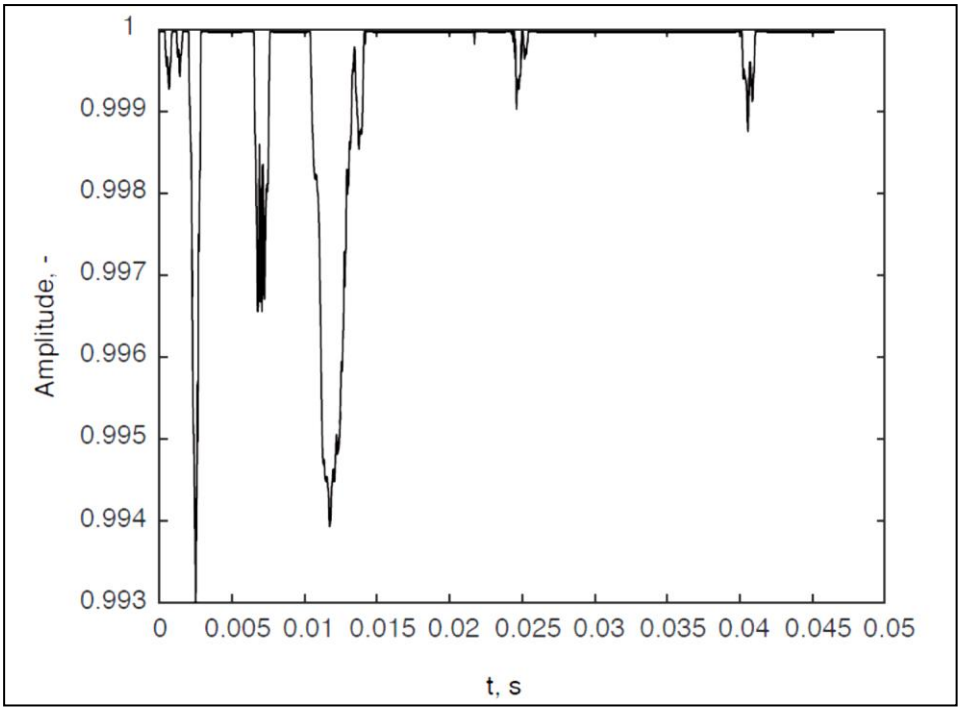

Figure 4.3: Acoustic signal for about 0.5 s from the start of signal captured.

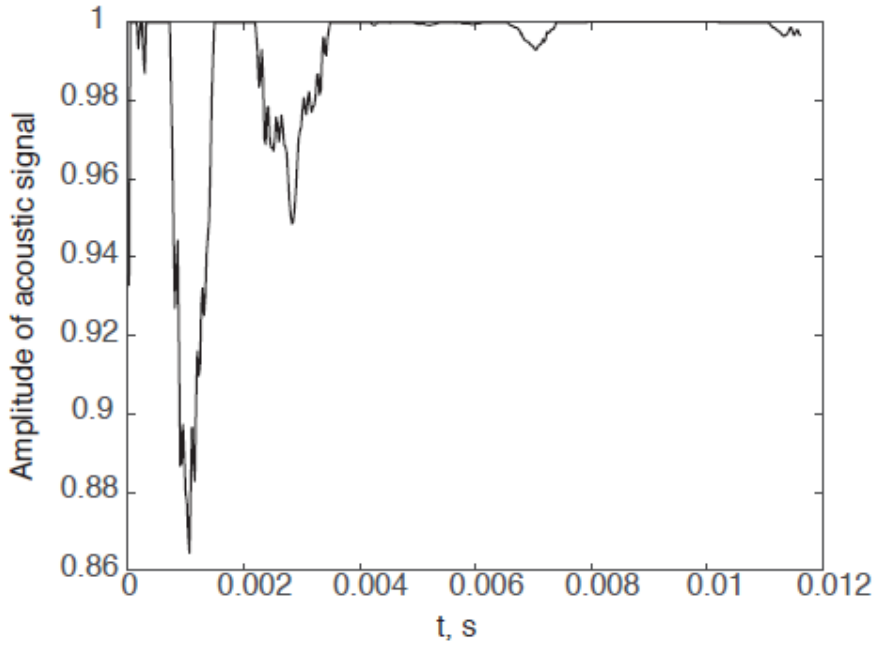

Figure 4.4: Acoustic signal for about 0.01 s from the start of signal captured.

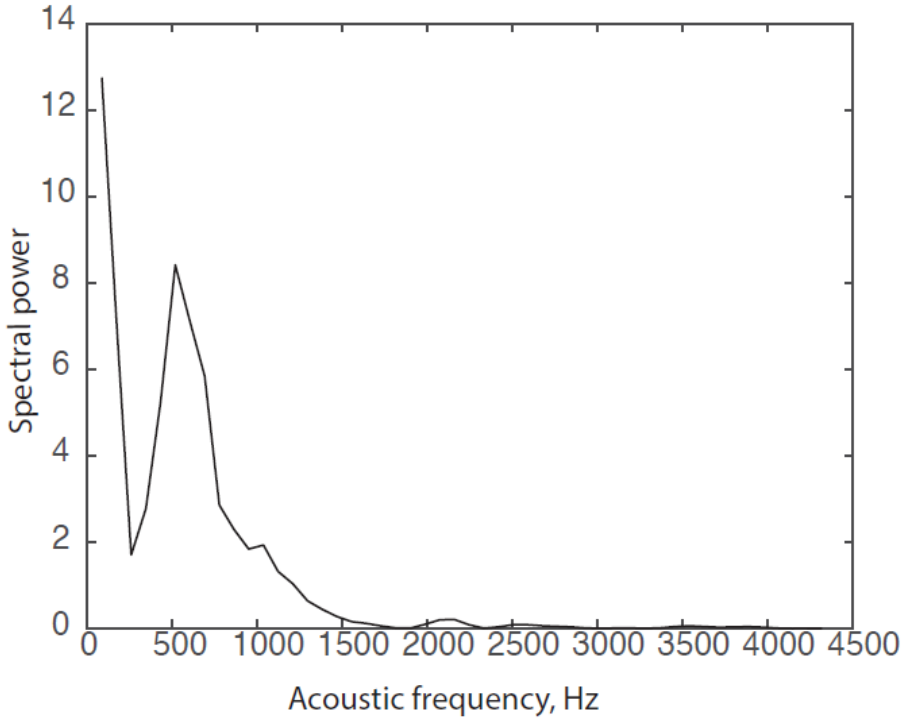

Figure 4.5: Fast Fourier transform of Acoustic signal presented in Figure 4.4.

4.2 Acoustic Signal in Bubble Column:

Acoustic signals in bubble column have several frequencies corresponding to bubbles of different sizes. A methodology to count bubble of various sizes and their classification was developed and used to get Bubble-Size Distribution (BSD). It is discussed in the following section.

4.2.1 Analysis of Acoustic Signal:

Acoustic signals were analysed using short-term Fourier Transform as a multi-resolution technique. The acoustic signals were cropped to 2048 (=2^{11}) data-points with no overlapping of data between two successive cropped signals. This cropped acoustic signal corresponds to 46.4 ms. Duration of the cropped signal was chosen after several trials so that only few (rarely more than 5) clear peaks could be clearly identified. A typical sample of cropped acoustic signal for U_g = 0.00833 m s^{-1}, Z = 0.05 m, H_s = 0.24

m for air-distilled water system is presented in Figure 4.6. It may be noted that the mike is not capturing the sounds of all bubbles present in the column, but it captures sound generated by bubbles in the vicinity of mike. Single bubble studies provided experimental proof that mike is capturing only acoustic signal generated in its close proximity. Thus the mikes mounted at different heights are providing acoustic signals at various vertical positions near to column wall. Since the mike was placed away from the top surface and the distributor, the acoustic signal may be expected to be free from the activities near the top liquid surface and the gas distributor.

Acoustic signal was analysed in the following manner.

(i) The acoustic signal measured at 44100 Hz as 'wma' files were converted to 'wav' file and stored in this format. The signal was read and cropped as non-overlapping sequential sets of 2048 data points each. Each audio segment corresponds to 0.0464 s, during which not more than 4 to 5 bubbles were present.

(ii) Matlab's 'fft' function was used for each such acoustic segment. The peaks in signal were determined using Matlab's 'fndpeak' function with peaks separated by 100 data points.

(iii) The signal has low (<200 Hz) and high frequency components which were not considered due to unrealistic bubble size not confirmed visually. High frequencies may be due to turbulence etc. Bubbles of 0.5 mm corresponding to high frequencies were discarded. Low frequency signal may be due to hydrodynamics process such as fluctuation of the liquid height and hence discarded.

(iv) The bubble diameter, d_b, corresponding to each frequency was determined. Since, while obtaining value of d_b, low frequencies were discarded, bubble size smaller than 0.0005 m were not considered. When bubble-size distributions were obtained using MATLAB's 'histogram' command with 25 equally spaced bins it was

observed that the function divided the data between naximum and minimum diameter. Therefore, the each class was not same in all cases. This procedure gave the values of minimum and maximum values of d_b. Therefore, code was written to separate different size group separated by 0.0005 m. The bubble size distribution (BSD) is plotted between numbers of bubble, N_b, as a function of bubble diameter, d_b, thus obtained.

Fourier transform of the cropped sample were determined. Fourier transform of a sample for U_g = 0.1 m s^{-1}, Z= 0.1 m, H_s = 0.2 m for air-distilled water is presented in Figure 4.8. At least two frequencies are clearly visible. Various frequencies separated by 100 points (= 2.27 ms) were determined using MATLAB's 'findpeaks' function.

Bubble-size was determined from the frequency at which the peaks are observed using Equation (2.11) developed by Minnaerf, referred by Strasberg (1956). The acoustic technique is based on the concept that natural frequency of sound generated by simple volume pulsation is given by Equation (2.11). For air-water system at atmospheric pressure f_0R = 330 cm/s. It was pointed out that only volume pulsation is to be considered since it diminishes very fast as the distance decreases.

4.3 Bubble Size Distribution (BSD):

Time of arrival of the bubbles was taken as to occur at the centre of the cropped sample. These values for the entire sample were stored in a single text file in the sequence in which the acoustic signal was cropped. The frequencies corresponding to bubbles diameter smaller than 0.0005 m were not considered as it may be superimposed by turbulence in the bubble column.

It must be clearly stated that since the mikes used did not recorded sounds produced by all the bubbles at any time but recorded sounds over a period of time different than average residence time of bubbles, the number of bubbles do not

represent the total number of bubbles present in the column at any time. However, it allows us to estimate BSD and Sauter-mean bubble diameter, d_{32}, based on number of bubbles counted at any location. Interfacial area was estimated from d_{32}. Al-Masry (2006) has pointed out that it is not possible to record true number of bubbles at any time.

The value Z = 0.00 m corresponds to a location at the air sparger. If the value of Z was less than the expanded bed height, then the mike was not always immersed in the liquid hence such data were discarded. It happened at low values of U_g for H_s < 0.2 m. At high values of U_g and for H_s < 0.2 m if the expanded bed height, H_e, was always greater than 0.2 m, then in some of the situations the mike captured acoustic signal in the foaming region.

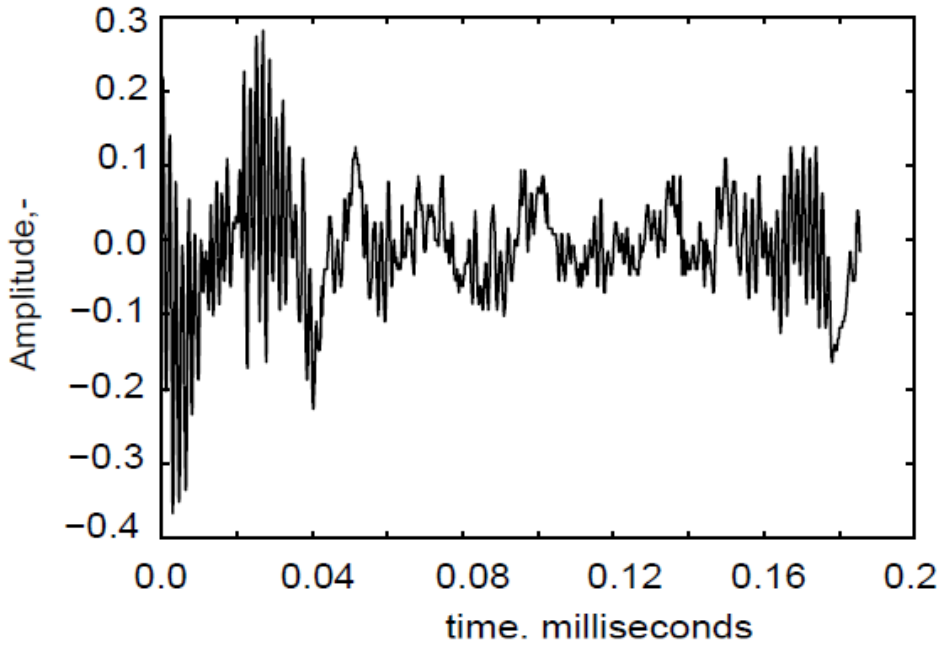

Figure 4.6: A typical cropped acoustic signal in bubble column at U_g = 0.00833 m s^{-1}, Z = 0.05 m, H_s = 0.24 m.

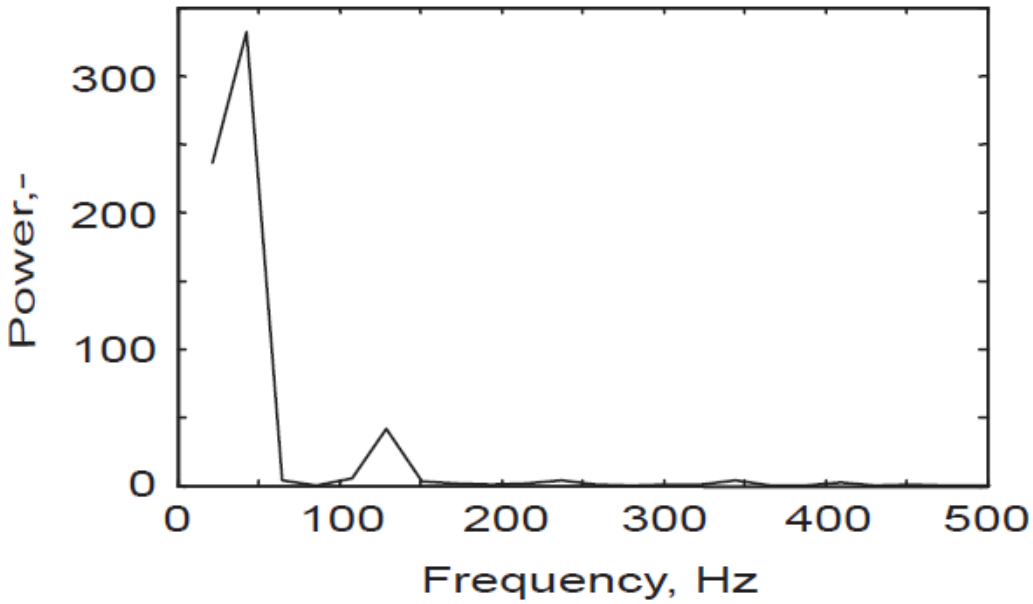

Figure 4.7: Fourier transform of cropped acoustic sample for U_g = 0.0083 m s^{-1}, Z = 0.05 m, H_s = 0.24 m.

4.3.1 BSD for Distilled Water:

Since the condenser mike used in the present study measured local acoustic signals. It was possible to study the effect of height above the distributor plate on BSD and other bubble characteristics. While obtaining bubble diameter, d_b, low frequencies were discarded as they might be due to process other than volume pulsation of bubbles. As a result of these, BSD plots do not show any bubble smaller than 0.0005 m.

BSD for distilled water at superficial air velocity, U_g = 0.0083 m s^{-1} and static bed height, H_s = 0.24 m for mike position, Z = 0.10 m is presented in Figure (4.8). It can be observed that most of the bubbles are of the size about 0.002 m. Some large bubbles up to a diameter of 0.005 to 0.012 m are also present. Thus, it is not the case of uniform bubbling. It may be termed as non-uniform homogeneous flow regime. The observations were verified by photographic method. The value of d_o is 0.0015 m, Bubbles larger of this size or of slightly large size are those who did not experience

bubble coalescence. Presence of large size indicates that bubble-coalescence is present. BSD is not single modal and hence fitting a single modal such as log-normal distribution is not proper.

4.3.1.1 Effect of U_g:

BSD at H_s = 0.22 m, Z = 0.00 m and for 0.0083 m $s^{-1} \leq U_g \leq$ 0.050 m s^{-1} is presented in Figure (4.9) to exhibit the dependence of U_g on BSD. It clearly shows that the bubbles formed are not of equal size. The sparger used in the present study did not have nozzles or had holes of same size. It was constructed by placing glass beads on perforated plate and with a top of wire mesh. The presence of bubbles smaller than 0.0015 m is clear indication that bubble break is dominating. Bubble coalescence is very few in number. The striking feature is that the bubble size distribution is unaffected by the superficial gas velocity.

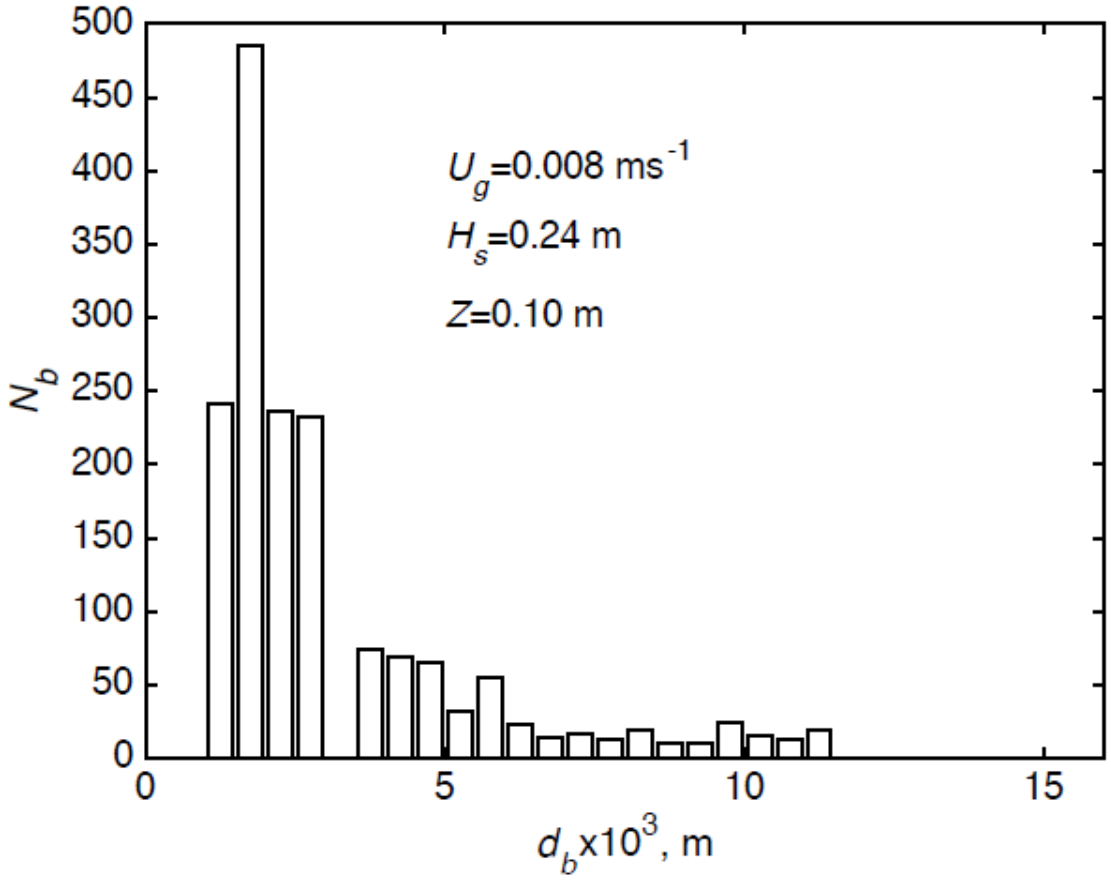

Figure 4.8: BSD for distilled water at U_g = 0.00833 m s^{-1}, H_s = 0.24 m, Z = 0.10 m.

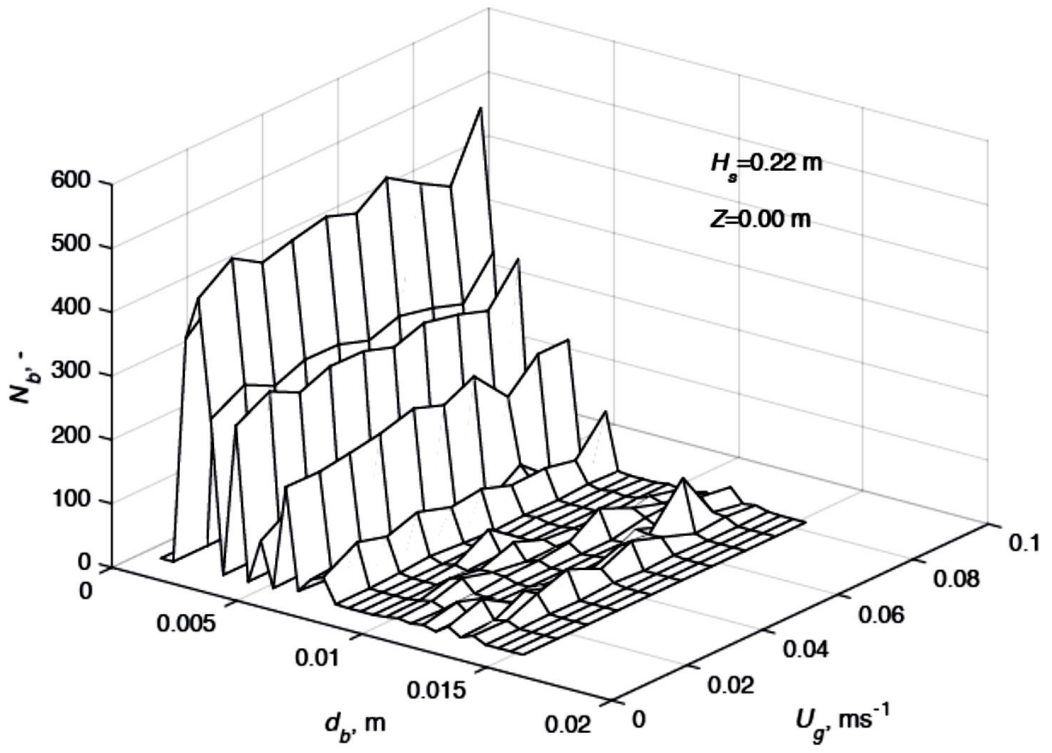

Figure 4.9: Effect of U_g on BSD for distilled water at H_s = 0.22 m, Z = 0.00 m.

To understand flow structure in the middle portion of the bubble column, BSD at H_s = 0.22 m, Z = 0.10 m is presented in Figure (4.10). From the visual observation it was confirmed that the position of the mike was not in the foaming region. The nature of BSD at all values of U_g is similar. The number of bubbles increased slightly with increasing values of U_g. However, the BSD is quite similar to that observed near the sparger (Z = 0.00 m). It suggests that bubble coalescence is absent for air-water system at all values of U_g. The flow regime is close to uniform bubbling regime. It may be termed as 'pseudo uniformly distributed' or 'non-uniform homogeneous regime' No significant bubble coalescence. A large number of bubbles have d_b < 0.0015 m, indicating that bubble breakup dominates at all values of U_g.

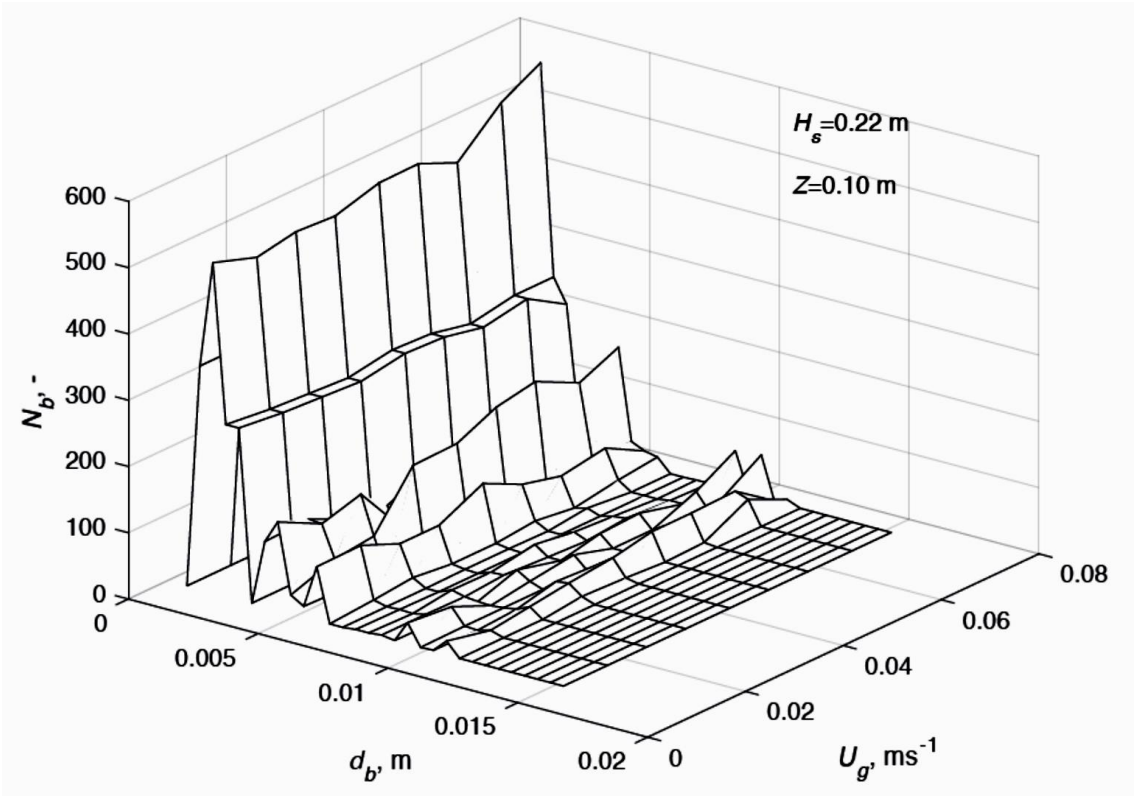

Figure 4.10: Effect of U_g on BSD for distilled water at H_s = 0.22 m, Z = 0.10 m.

4.3.1.2 Effect of H_s:

BSD at U_g=0.033 ms^{-1}, Z = 0.00 m and 0.16 m $\leq H_s \leq$ 0.24 m is presented in Figure (4.11). The BSD is similar at all values of H_s. Few large bubbles having bubble diameter = 0.010 m can be seen in the figure. The natute of BSD is similar in all cases. It is expected since the formation of bubble is not affected much due to static bed height. The bubble coalescence is absent.

BSD at U_g=0.017 ms^{-1}, Z = 0.20 m and 0.16 m $\leq H_s \leq$ 0.24 m is presented in Figure (4.12). No effect of H_s on BSD is visible. However, number of large bubbles are lesser than that shown in Figure (4.11).

4.3.1.3 Effect of *Z:*

BSD at U_g=0.042 ms^{-1}, H_s=0.20 m and 0.00 m $\leq Z \leq$ 0.02 m is presented in Figure (4.13). The BSD becomes narrow as the value of Z increased. The maximum value of d_b sharply decreases from 0.015m to 0.007m as Z increases from 0.00 m to 0.20 m. It clearly indicates occurrence of bubble breakup in the upper portion of the column at a particular value of H_s and U_g. However, it is difficult to clearly specify any value of H_s and U_g at which significant bubble coalescence is observed. This behavior was observed in all runs. It may be noted that the location of foam layer above the sparger changes when the expanded bed height changes as a result of change of H_s and U_g but the locations of mikes do not change.

At all values of H_s, U_g and Z very few large bubbles were present for air-water system indicating uniform bubbling regime. At high air velocity, bubble coalescence might have taken place in the upper region, where bubble breakup is prominant.

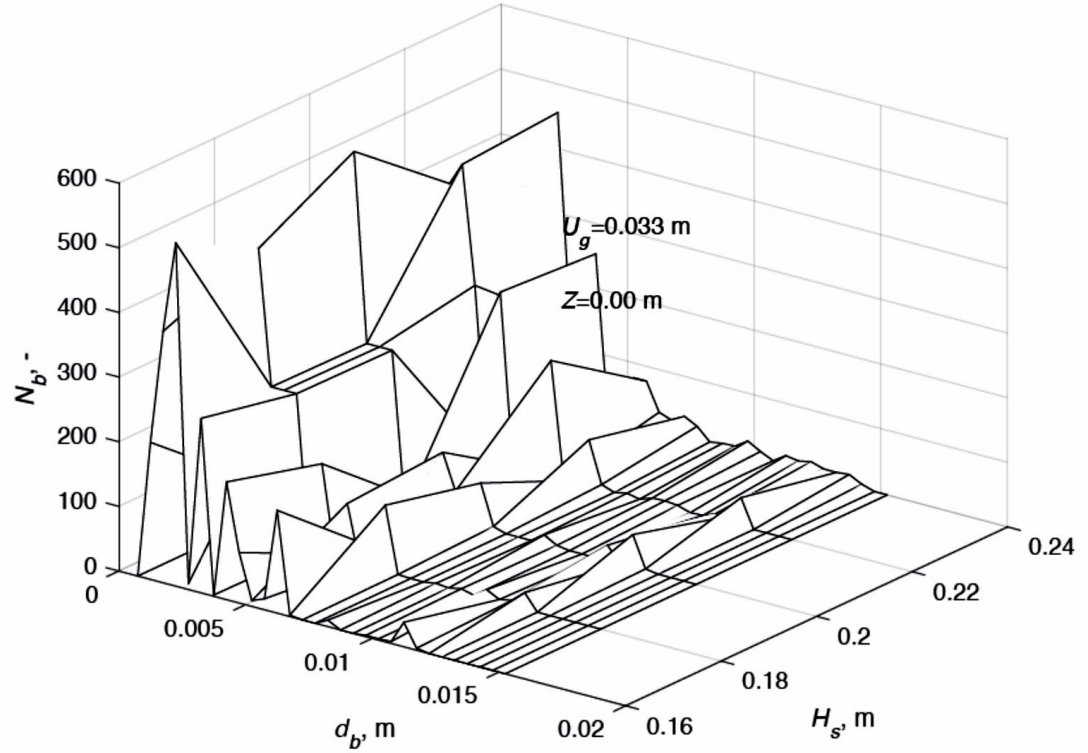

Figure 4.11: Effect of H_s on BSD for distilled water at Z = 0.00 m, U_g = 0.033 ms^{-1}.

The number of bubble sizes is not changing even if the value of U_g increases. It seems that the bubbles surrounding the mike acts as sound absorber and reduces the distance upto which the mike can capture the acoustic measurement.

The microphones used at different vertical distane from the sparger captured the change in bubble size. However, it should be interesting to study the other liquid systems.

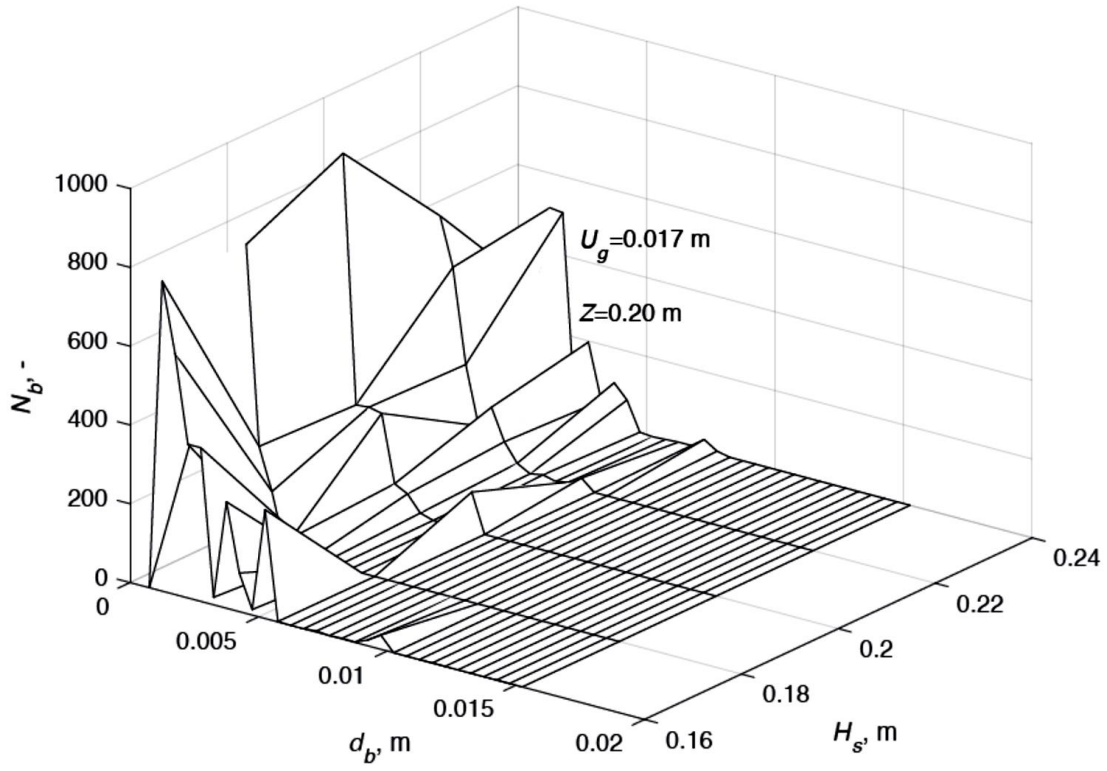

Figure 4.12: Effect of H_S on BSD for distilled water at Z = 0.20 m, U_g = 0.017 ms^{-1}.

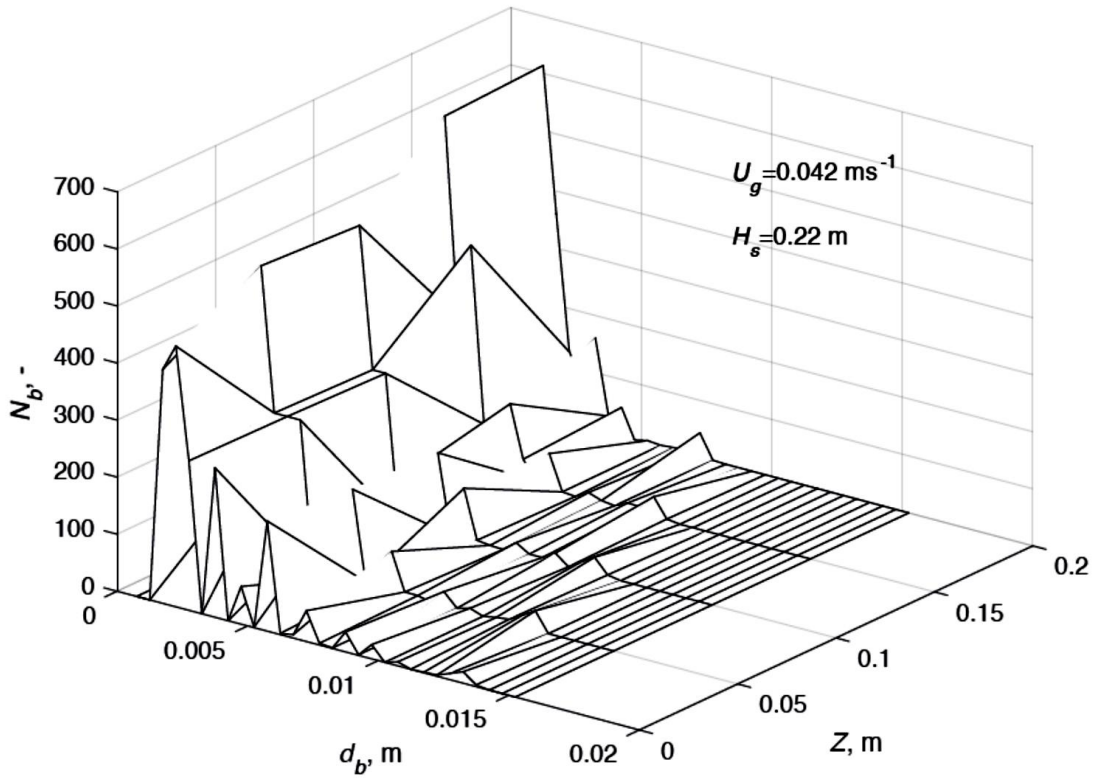

Figure 4.13: Effect of Z on BSD for distilled water at H_S = 0.20 m, U_g = 0.042 ms^{-1}.

4.3.2 BSD for Ethylene Glycol solution

To study the effect of viscosity in a Newtonian fluid on bubble behaviour an aqueous solution of ethylene glycol (EG) was used. The bubble-size distribution for 0.5 wt % EG soln. at superficial air velocity, U_g = 0.222 m s^{-1}, static bed height, H_S = 0.20 m and for values of Z = 0.15 m are presented in Figures (4.14). The BSD shows that the bubble size varies smoothly in contrast to the case of distilled water for which bubble size were of two distinctly different classes. The largest bubble size is about 0.010 m while in case of distilled water bubbles as large as 0.015 m were observed. It indicates that bubble breakup dominates. Bubble coalescence is lesser than that in case of air-water. EG acts as coalescene inhibitor.

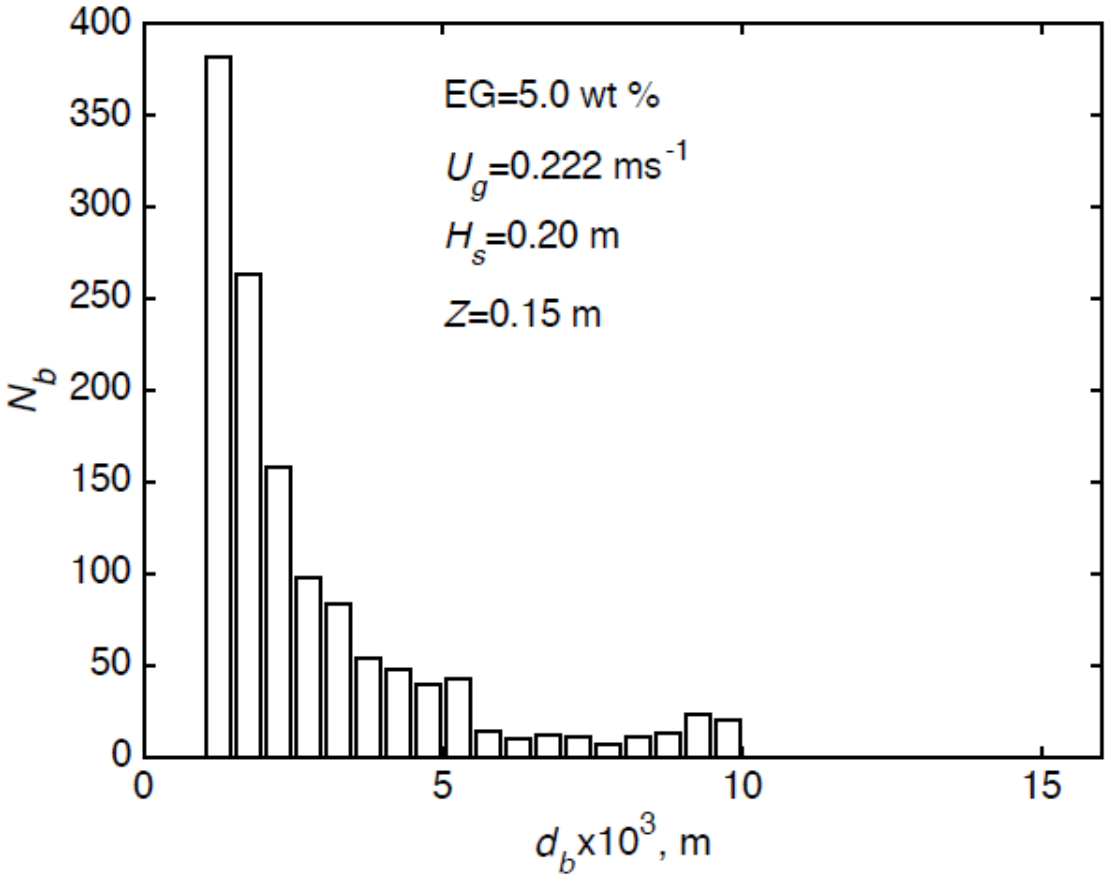

Figure 4.14: BSD for 0.5%(w/w) ethylene glycol solution at U_g = 0.0083 ms^{-1}, H_s=0.15 m and Z=0.00 m.

4.3.2.1 Effect of U_g:

BSD for 0.5% (w/w) Ethylene Glycol solution in water at H_s = 0.10 m, Z = 0.00 m and for 0.056 m s^{-1} ≤ U_g ≤ 0.222 m s^{-1} is presented in Figure (4.15) to exhibit the dependence of U_g on BSD. Bubbles are not of equal size and follow a smooth variation of bubble size. As the value of U_g increases the number of bubbles increases slightly. The flow regime is clearly not uniform. This trend is observed in all cases.

4.3.2.2 Effect of H_s:

BSD for 0.5% (w/w) Ethylene Glycol solution in water at U_g=0.111 ms^{-1}, Z = 0.05 m and 0.1 m $\leq H_s \leq$ 0.2 m is presented in Figure (4.16). As value of H_s increases, number of small bubbles increases. Large bubbles also appeared at high values of H_s. It is expected since at high static bed height the bubbles have a large path and hence find more time for bubble coalescence and bubble breakup phenomena to take place.

4.3.2.3 Effect of *Z:*

BSD for 0.5% (w/w) Ethylene Glycol solution in water at U_g=0.139 ms^{-1}, H_s=0.10 m and for 0.00 m $\leq Z \leq$ 0.02 m is presented in Figure (4.17). The BSD becomes narrow as the value of Z increased. The maximum value of d_b sharply decreases from 0.010m to 0.005 m as Z increases from 0.00 m to 0.20 m. It clearly indicates occurrence of bubble breakup in the upper portion of the column at a particular value of H_s and U_g. The static bed height is 0.1 m and the mike at 0.02 m is in the foam region. The decrease of bubble size shows the bubble size in the structured foam.

This behaviour was observed in all runs. It may be noted that the location of foam layer above the sparger changes when the expanded bed height changes as a result of change of H_s and U_g but the locations of mikes do not change.

BSD becomes narrow as the value of Z increases. The trend is very similar to that observed in case of distilled water. While in the case of distilled water there were very few large bubbles, in case of EG solution the large bubbles were many. The bubbles observed in case of 5% EG solution were larger than that observed for 0.5 wt % EG solution. Otherwise all other feature same. The BSD for 5%(w/w) EG solution is not presented here for the reason that BSD for water and EG solution were for different range of U_g and hence data for 0% EG solution i.e. for distilled water are not measured.

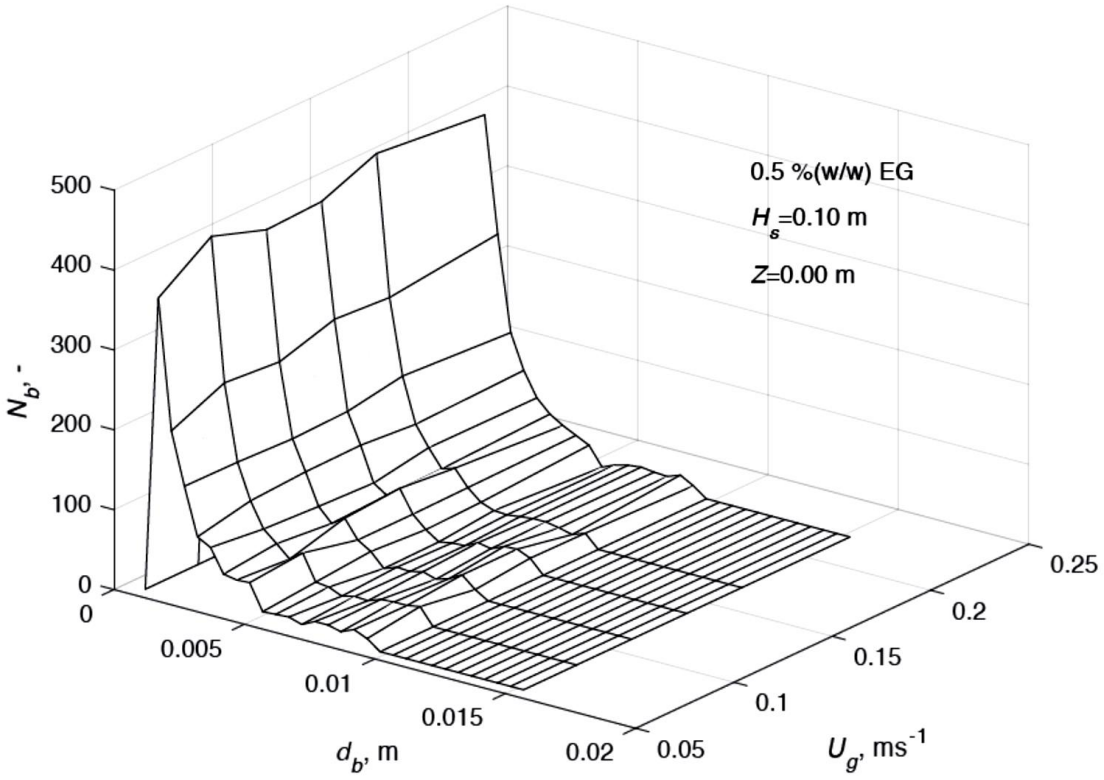

Figure 4.15: Effect of U_g on BSD for 0.5% EG solution at H_s = 0.10 m, Z = 0.00 m.

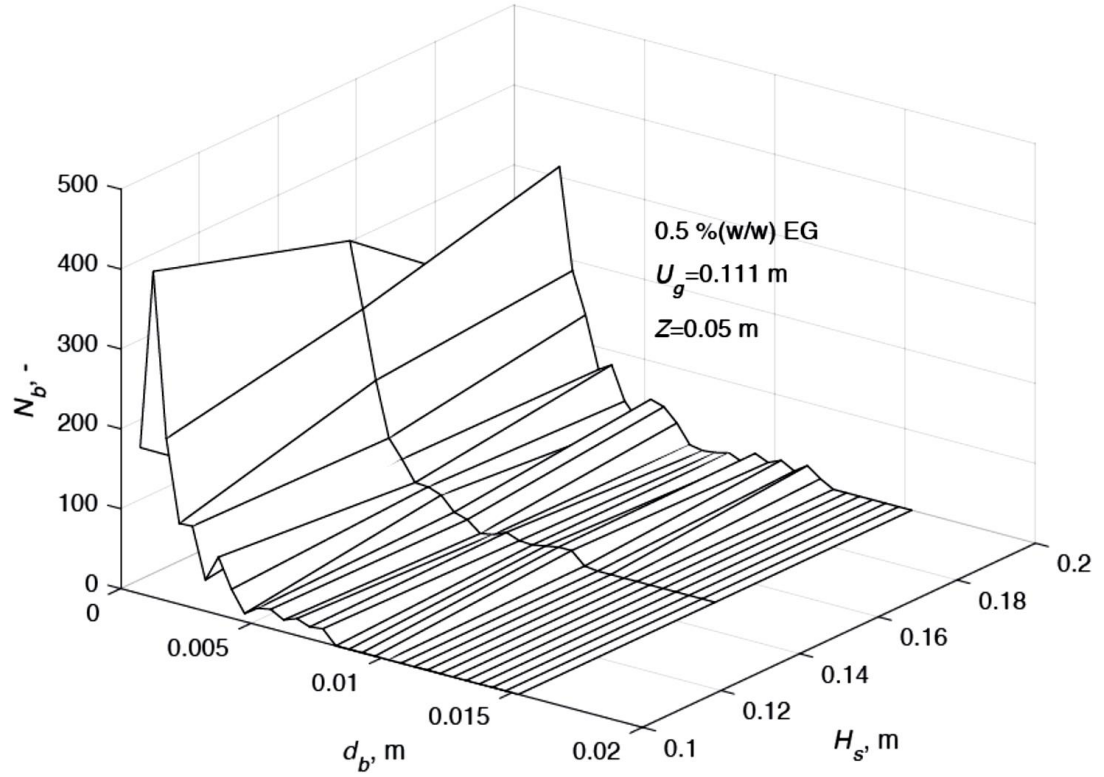

Figure 4.16: Effect of H_s on BSD for 0.5% EG solution at U_g = 0.111 ms^{-1}, Z = 0.05 m.

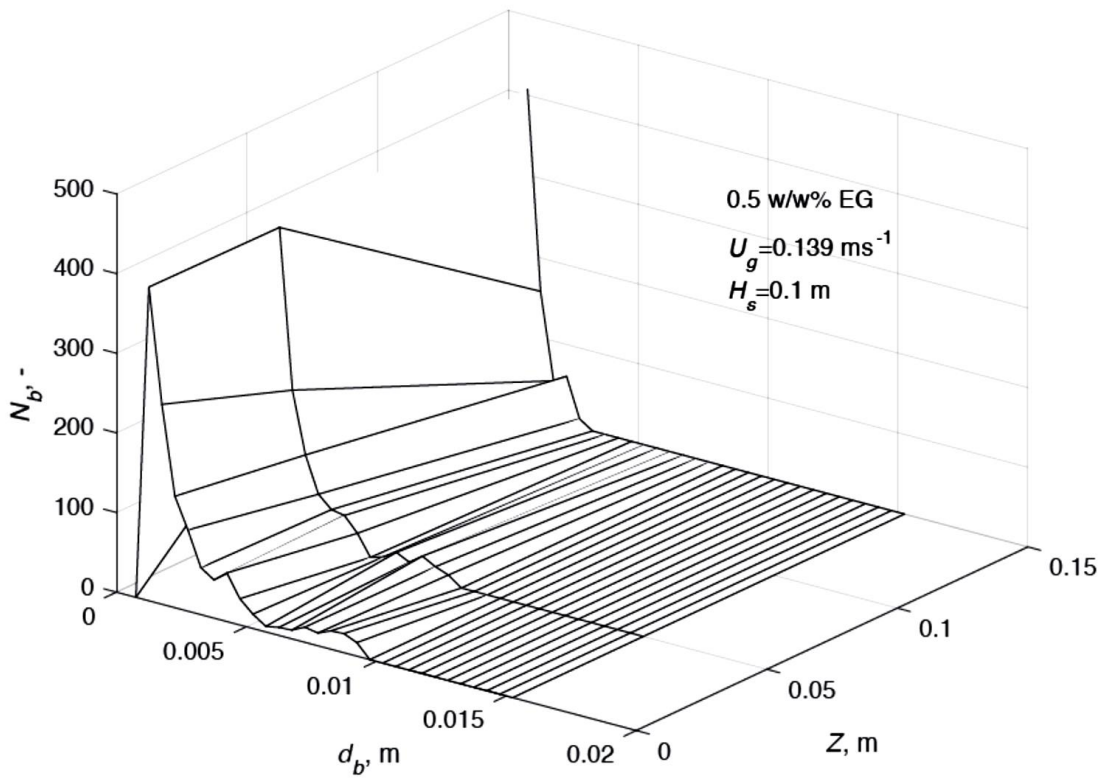

Figure 4.17: Effect of Z on BSD for 0.5% EG solution at H_S = 0.10 m, U_g = 0.139 ms^{-1}.

4.3.3. Bubble-Size Distribution for air/CMC Solution (aq.) system:

Aqueous solution of CMC behaves as power-law fluid. The bubble behaviour is expected to be different than that observed for air/water system. BSD for 0.1%(w/w) CMC solution at U_g = 0.0417 ms^{-1}, H_S=0.15 m and Z=0.00 m is presented in Figure 4.18. Three different class of bubbles, small bubbles in the size range of 0.001 to 0.003 m, middle size bubbles in the range of 0.0035 to 0.006 m and large bubbles of size 0.007 to 0.012 m are observed. It is in contrast to observations in case of EG solution. BSD is multi modal and may be result of bubble coalescence taking place.

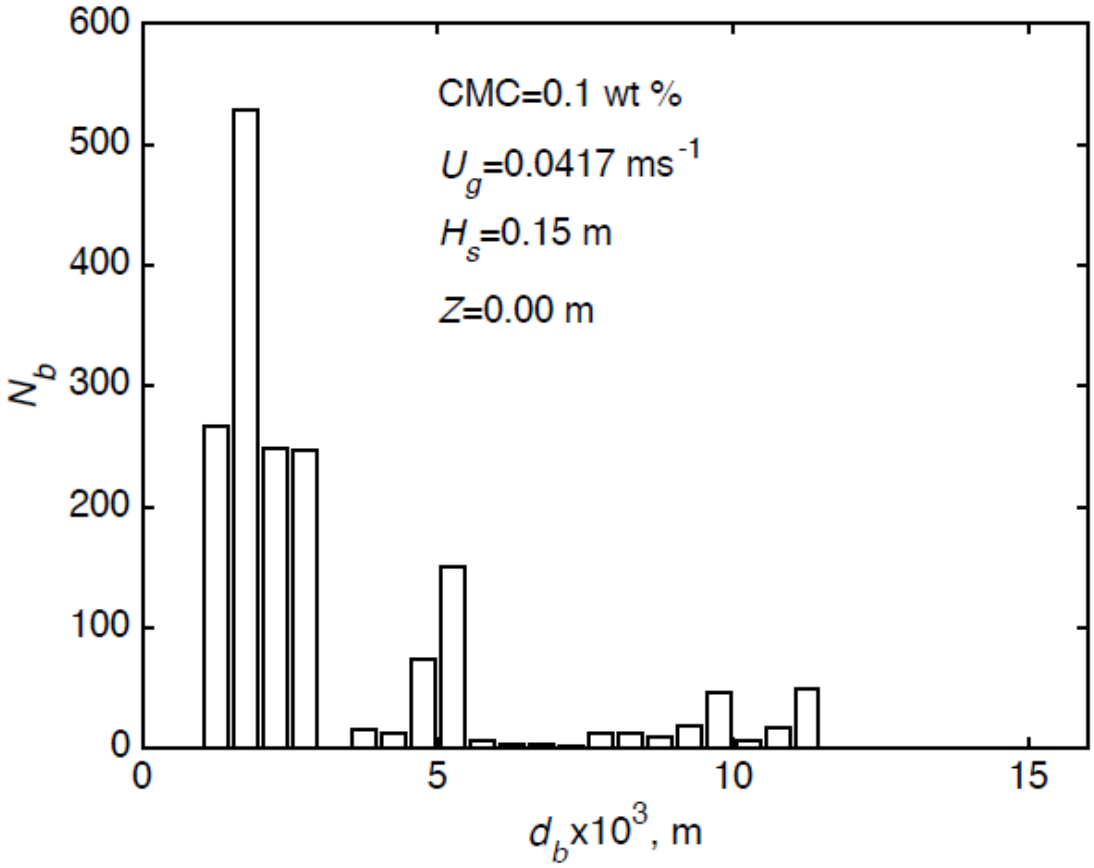

Figure 4.18: BSD for 0.1%(w/w) CMC solution at U_g = 0.0417 ms^{-1}, H_s=0.15 m and Z=0.00 m.

4.3.3.1 Effect of U_g:

BSD for 0.1 wt % aq. Soln. of CMC at H_s = 0.15 m, Z = 0.05 m and 0.042 m s^{-1} ≤ U_g ≤ 0.167 m s^{-1} is presented in Figure (4.19). There are at least three groups of bubbles. The entire bubble population consists of a large group of bubbles of sizes 0.002-0.003 m, a small group of bubbles of diameter 0.004-0.005 m and few bubbles ranging in bubble diameter between 0.007- 0.010 m. At large values of U_g (> 0.083 m s^{-1} and above) bubble of diameter 0.025 m can also be seen. The flow regime does not belong to category of bubbling flow regime as the bubbles are of not uniform size. As expected the maximum bubble size increasing with increasing U_g.

4.3.3.2 Effect of *Z:*

BSD for 0.1 %(w/w) CMC solution at U_g=0.083 ms^{-1}, H_s=0.15 m and 0.00 m $\leq Z \leq$ 0.15 m is presented in Figure (4.20). Mike located at Z=0.2 was not properly submerged in the solution. As the distance above the sparger increased maximum size of d_b decreased from 0.0095 m to 0.0021 m. The value of d_b at Z=0.0 m is within 0.0093±0.0002 m at all values of U_g and H_s=0.15 m. It suggests that BSD near sparger is governed by the bubble formation phenomena. It indicates that bubble breakup for large bubbles takes place above the sparger. Possibly the static bed height was not enough to provide sufficient time to upward moving bubbles for coalescence. The trend is similar to that observed in air-water system. The number of intermediate size bubbles increases with increasing Z.

4.3.3.3 Effect of H_s:

BSD for 0.1 (w/w)% CMC soln. at U_g=0.042 ms^{-1}, Z=0.15 m and H_s = 0.10, 0.15 and 0.20 m are presented in Figure (4.21). As the value of H_s increases from 0.10 to 0.20 m increased maximum size of d_b increased from 0.0079 m to 0.0123m. It seems that at large value of H_s bubbles get more time to coalesce. It is consistent with the observation that small bubbles coalesce to form large bubbles.

4.3.3.4 Effect of Concentration:

BSD for 0.1, 0.5 and 1.0 %(w/w) CMC in water and water (0%) at U_g=0.063 ms^{-1}, H_s=0.20 m and Z=0.05 m is presented in Figure (4.22). Three groups of bubbles of diameter of about 0.002, 0.005 and 0.010 m are observed. Large bubbles were few. Multi-modal probability BSD was observed in all other cases. Surprisingly no significant effect of concentration on BSD is observed.

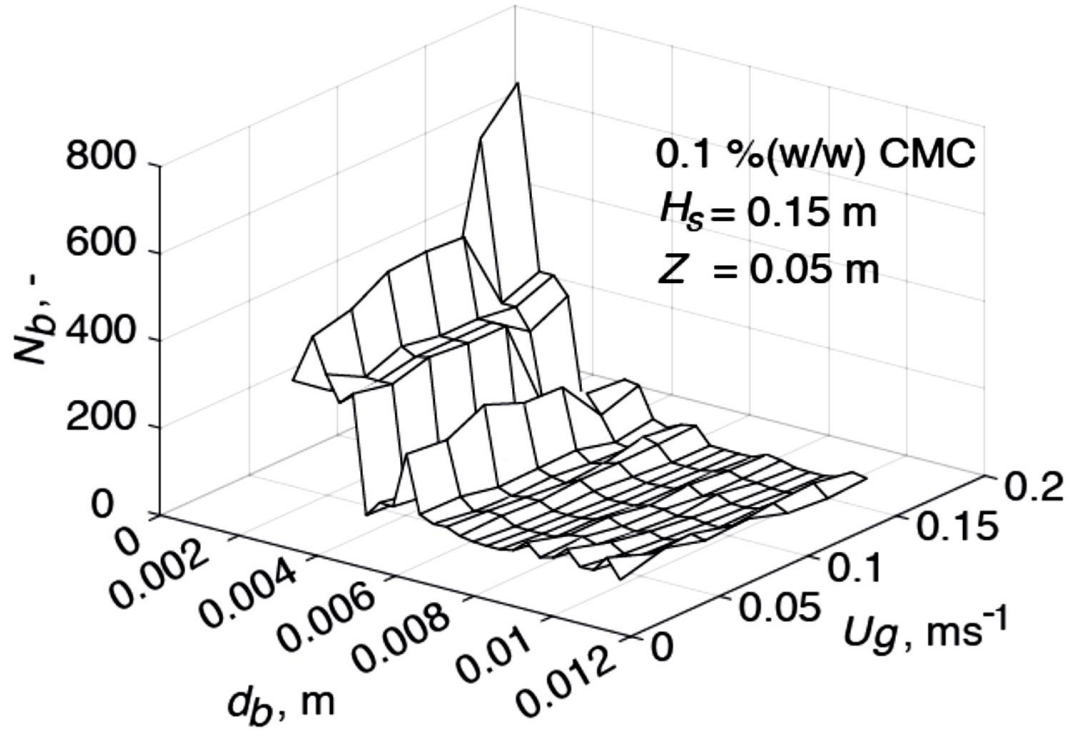

Figure 4.19: Effect of U_g on BSD for 0.1 % (w/w) CMC soln. at H_s =0.15 m and Z=0.05 m.

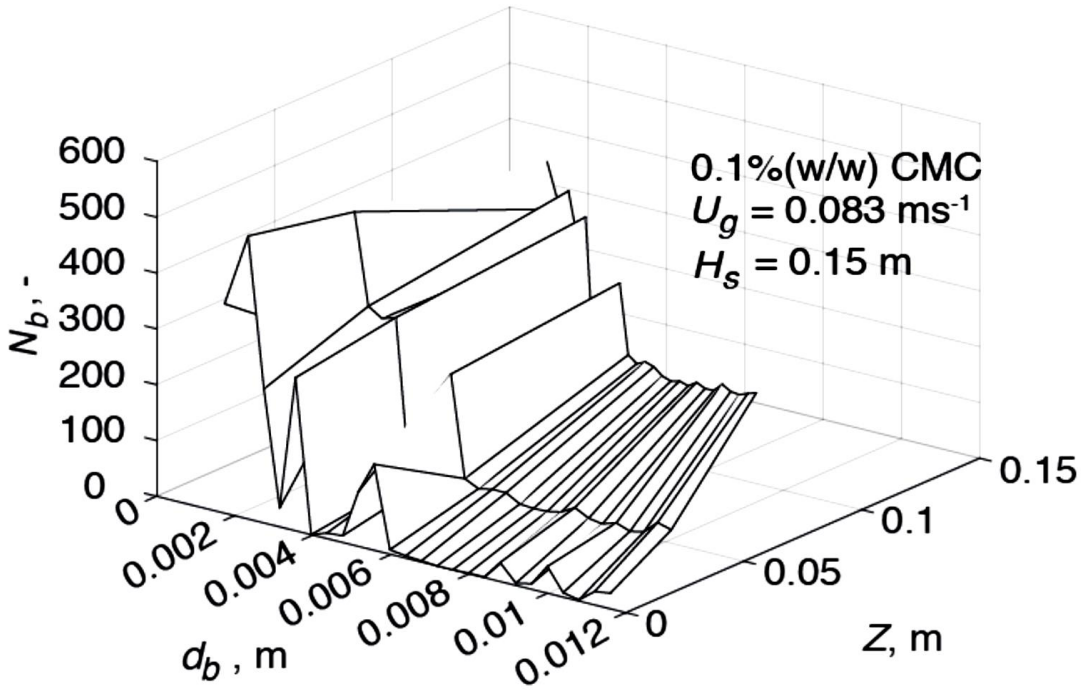

Figure 4.20: Effect of Z on BSD for 0.1 % (w/w) CMC soln. at U_g=0.083 ms^{-1} and H_s=0.15 m.

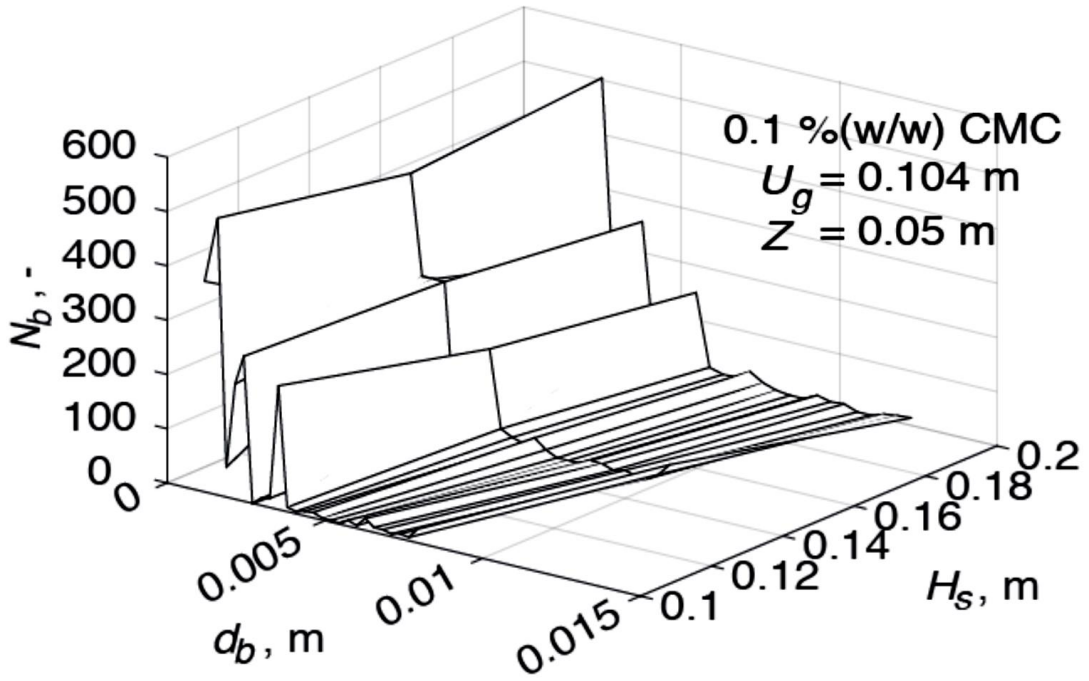

Figure 4.21: Effect of H_s on BSD for 0.1 % (w/w) CMC soln. at U_g=0.104 ms^{-1} and Z=0.05 m.

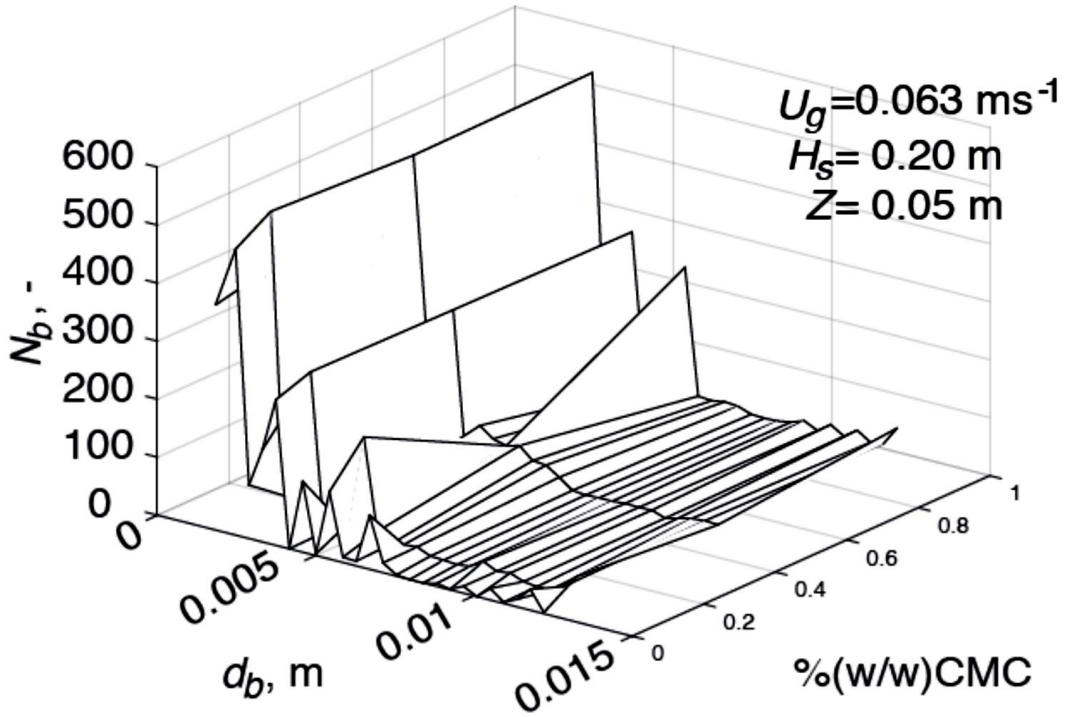

Figure 4.22: Effect of conc. on BSD for air/aq. CMC soln. at U_g=0.063 ms^{-1}, H_s=0.20 m and Z=0.05 m.

4.3.4 BSD for NaOH solution:

NaOH was used as an electrolyte. BSD for 0.1 wt % NaOH soln. at U_g = 0.0625 m s^{-1}, H_s = 0.15 m and Z = 0.00 m is presented in Figure (4.23). The BSD is molti-modal and a log-normal fit or any other distribution is not appropriate. Bubble population consists of a three groups of bubbles of sizes 0.002-0.003 m, 0.004-0.006 m and 0.006-0.011 m. The number of small bubbles forms the largest group.

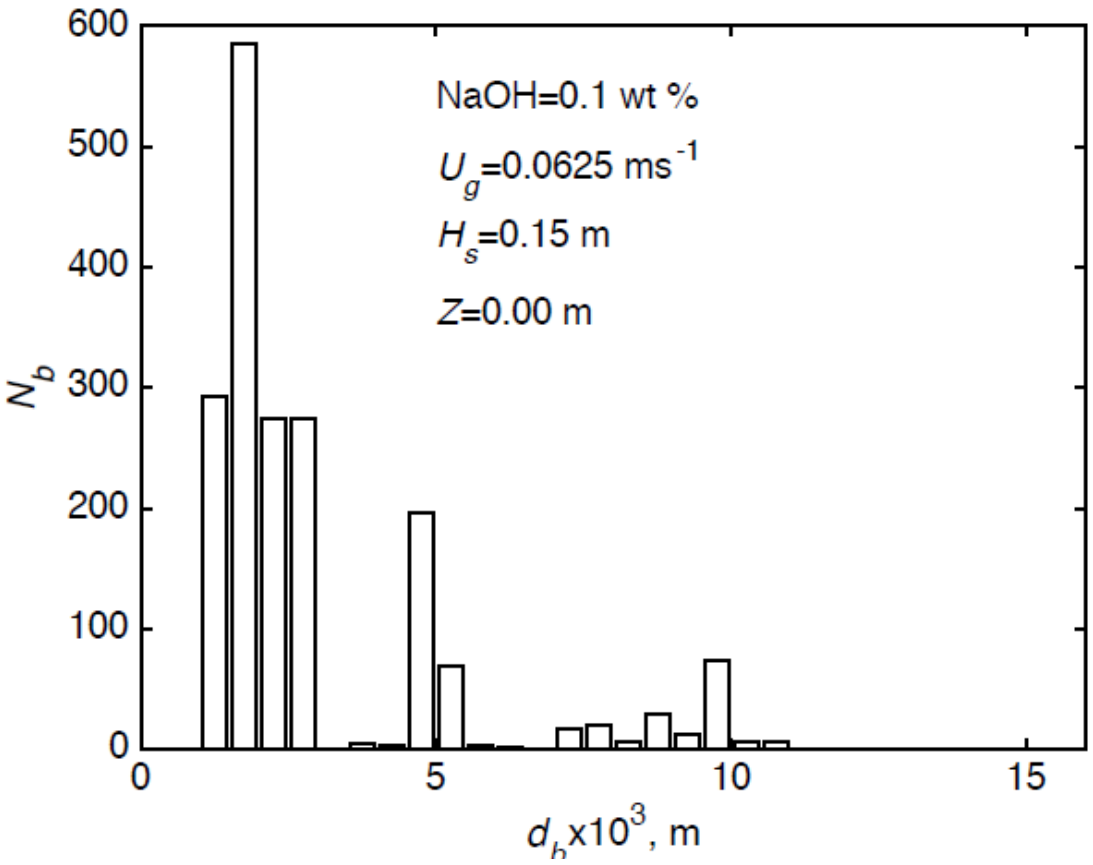

Figure 4.23: BSD for 0.1%(w/w) NaOH soln. at U_g = 0.0625 ms^{-1}, H_s=0.15 m and Z=0.00 m.

4.3.4.1 Effect of U_g:

BSD for 0.1 % (w/w) NaOH solution at H_s =0.10 m and Z=0.05 m 0.042 m $s^{-1} \leq U_g \leq$ 0.167 m s^{-1} is presented in Figure (4.24). There are mostly small bubbles of size 0.003-0.004 m. Only few large bubble bubbles are also observed. The same was observed visually also. The flow regime does not belong to category of uniformly bubbling flow regime as the bubbles are of not uniform size.

4.3.4.2 Effect of *Z:*

BSD for 0.1 % (w/w) NaOH soln. at U_g=0.0833 ms^{-1} and H_s=0.20 m and Z =0.00, 0.05 and 0.15 m is presented in Figure (4.25). Mike located at Z=0.2 was not properly submerged in the solution. As the value of Z increased maximum size of d_b decreased from 0.012 m to 0.007 m. It indicates that bubble breakup for large bubbles takes place above the sparger. Possibly the static bed height was not enough to provide sufficient time to upward moving bubbles for coalescence. The trend is similar to that observed in air-water system.

4.3.4.3 Effect of H_s:

BSD for 1.0 % (w/w) NaOH soln. at U_g=0.0625 ms^{-1} and Z=0.05 m and H_s = 0.10, 0.15 and 0.20 m is presented in Figure (4.26). As the value of H_s increases from 0.10 to 0.20 m increased maximum size of d_b increased from 0.008 m to 0.012 m. It seems that at large value of H_s bubbles get more time to coalesce. It is consistent with the observation that small bubbles coalesce to form large bubbles.

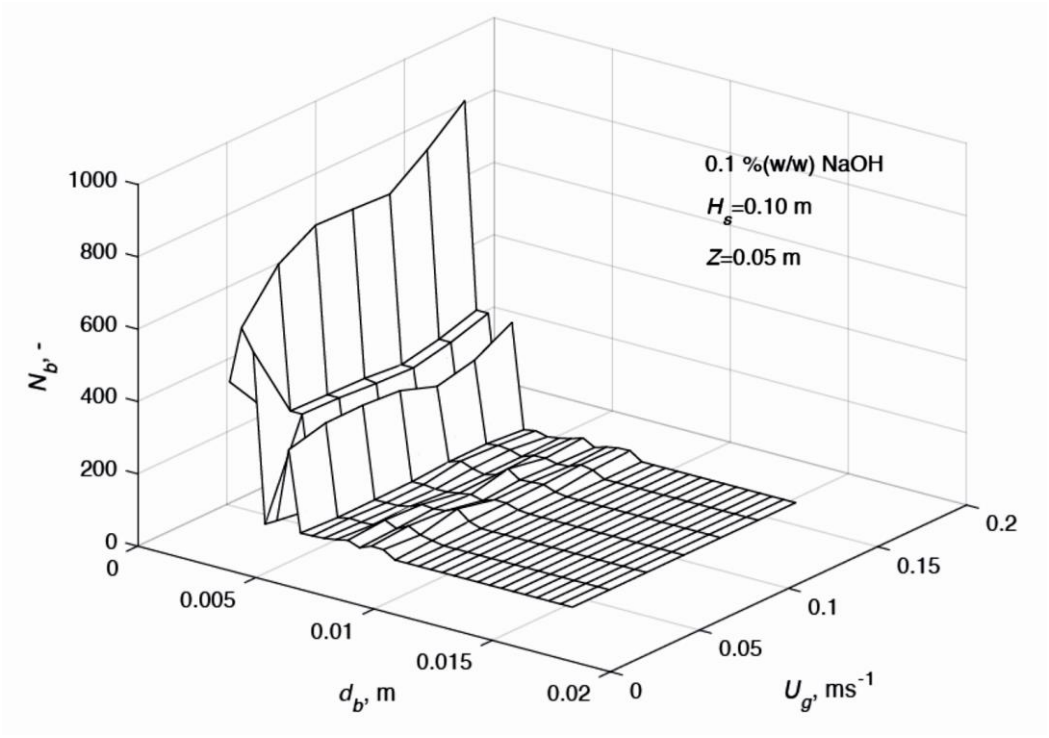

Figure 4.24: Effect of U_g on BSD for 0.1 % (w/w) NaOH soln. at H_s =0.10 m and Z=0.05 m.

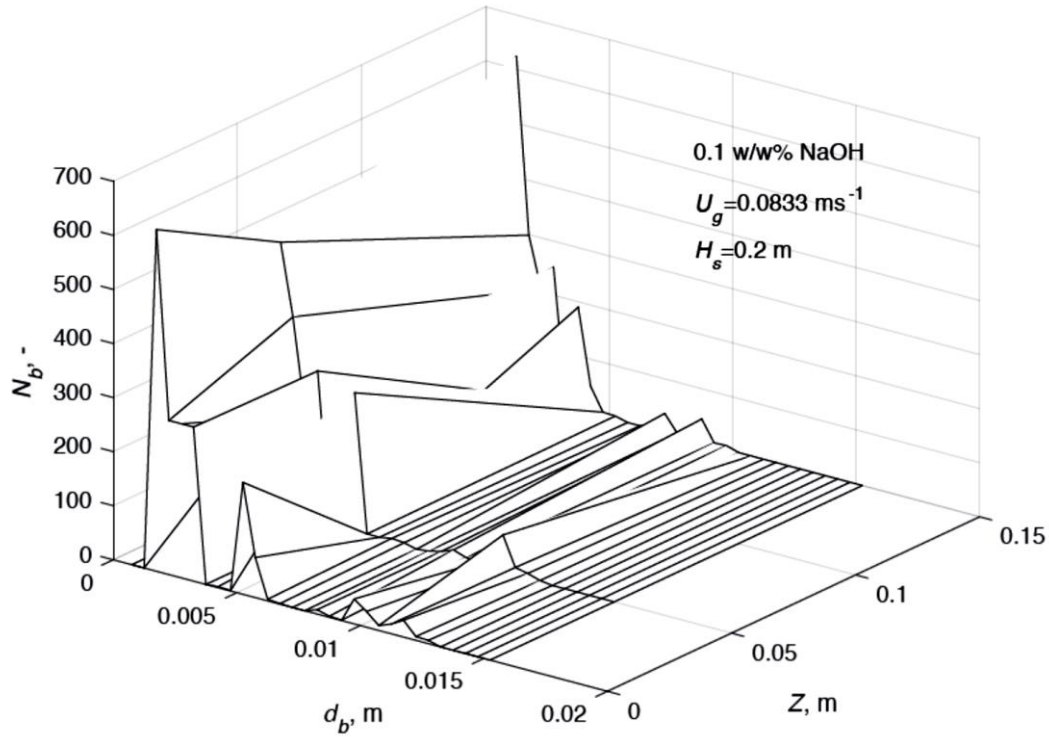

Figure 4.25: Effect of Z on BSD for 0.1 % (w/w) NaOH soln. at U_g=0.0833 ms^{-1} and H_s=0.20 m.

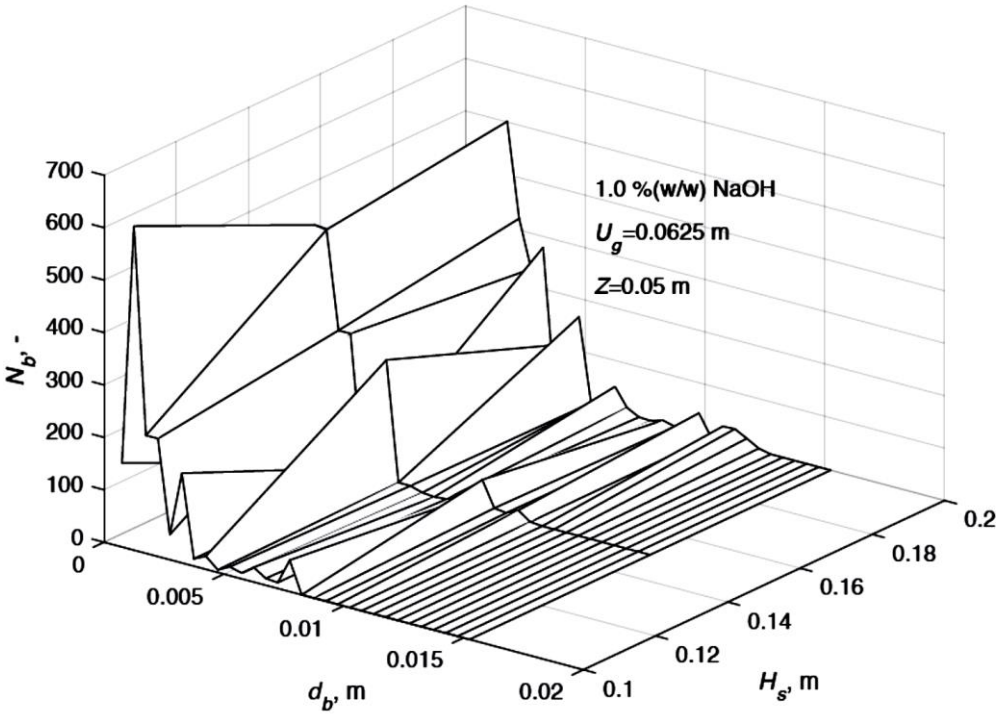

Figure 4.26: Effect of H_s on BSD for 1.0 % (w/w) NaOH soln. at U_g=0.0625 ms^{-1} and Z=0.05 m.

4.3.4.4 Effect of Concentration:

BSD for 0.1, 0.5 and 1.0 %(w/w) NaOH solution in water and water (0%) at U_g=0.0083 ms^{-1}, H_s=0.20 m and Z=0.05 m is presented in Figure (4.27). The bubbles are mostly tiny bubbles with few large bubbles. The number of large bubbles decreases as concentration of NaOH increases. Multi-modal probability BSD was observed at all operating conditions.

From the trends seen for all systems following conclusions may be drawn.

(i) The bubble-size distribution becomes narrow as the distance above distributor plate increases. It indicates occurrence of bubble breakup in the upper portion of the column. Recirculation of small bubbles in the wake created by large bubbles may be another reason.

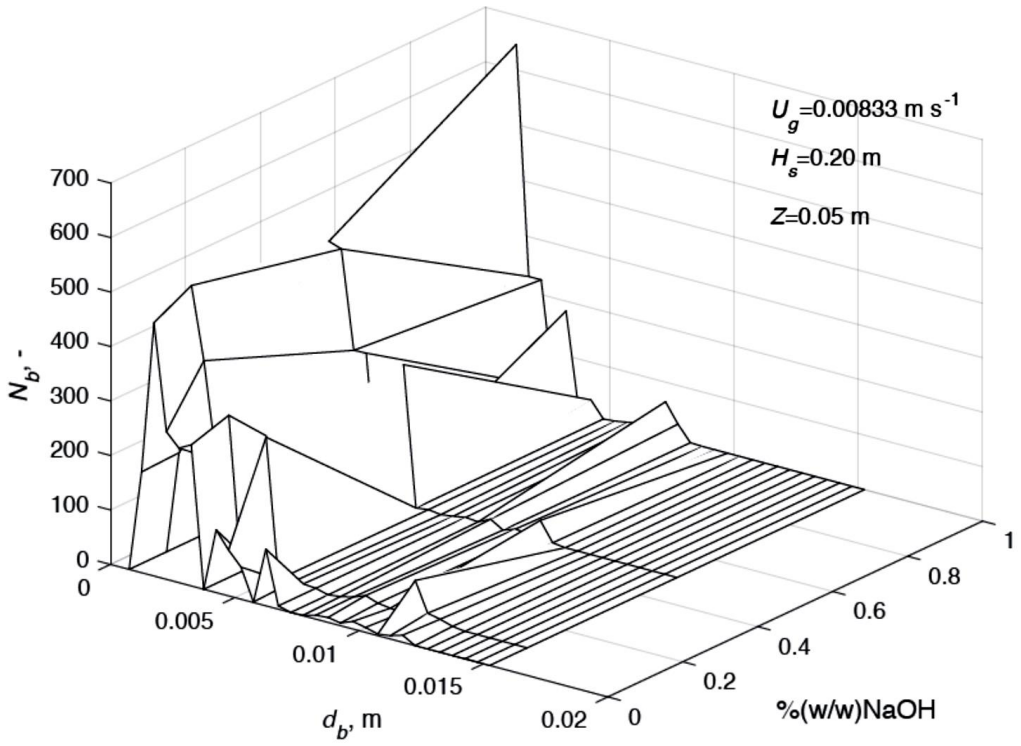

Figure 4.27: Effect of conc. on BSD for air/NaOH soln. at U_g=0.0083 ms^{-1}, H_s=0.20 m and Z=0.05 m.

(ii) Large bubbles were almost absent in air-distilled water system at low superficial air velocity indicating uniform bubbling regime. At high air velocity bubble coalescence takes place. From all the systems studied it may be concluded that bubble coalescence takes place in the lower region. In the upper portion of the column bubble breakup takes place.

(iii) In viscous fluid bubble coalescence is suppressed as is observed in case of air-EG soln. and air-CMC soln. systems.

(iv) Except for air-distilled water system multi-modal probability distribution were observed hence it is not possible to fit a simple probability function such as log-normal distribution in all cases.

4.4 Statistical Analysis of Bubble Size Distribution:

For quantitative description of the bubble-size distribution statistical analysis are required. In all four moments were considered.

Mean of the sample, $\bar{x}$, is arithmetic mean. It is estimated using the following formula.

$$\bar{x} = \frac{1}{n}\sum_{i=1}^{n} x_i \tag{4.1}$$

The mean was used to estimate other higher moments, however, in case of bubble size, Sauter mean diameter, d_{32}, is more meaningful as it can be used to estimate specific interfacial area of bubbles. It is easily estimated from the value of d_{32}. Interfacial area has been defined in literature by Equation (2.9) and (2.10).

Variance, σ, second moment about the sample mean is a measure of spread of the data. MATLAB's function 'var' was used to estimate variance. Variance of a sample is given by the following formula.

$$\sigma = \frac{1}{n-1}\sum_{i=1}^{n}\left(x_i - \bar{x}\right)^2 \tag{4.2}$$

Skewness, third moment around sample mean is a measure of asymmetry of the data around the sample mean. It was calculated using MATLAB's skewness function. By default, it does not correct bias and is given by

$$s_1 = \frac{\frac{1}{n}\sum_{i=1}^{n}\left(x_i - \bar{x}\right)^3}{\left(\sqrt{\frac{1}{n}\sum_{i=1}^{n}\left(x_i - \bar{x}\right)^2}\right)^3} \tag{4.3}$$

Kurtosis, fourth moment around sample mean is a measure of peakedness of the data around the sample mean. It determines how much outlier prone is the distribution. Since the normal distribution has a value of kurtosis equal to 3, any value

of kurtosis greater than 3 tells that the distribution is prone to outlier. It was calculated using MATLAB's kurtosis function which by default uses the following formula.

$$k_1 = \frac{\frac{1}{n}\sum_{i=1}^{n}\left(x_i - \bar{x}\right)^3}{\left(\frac{1}{n}\sum_{i=1}^{n}\left(x_i - \bar{x}\right)^2\right)^2} \tag{4.4}$$

4.4.1 Variance, σ, for air-water system:

Value of σ, for air-water system as a function of U_g, H_s and Z are presented in Figure (4.28). No definite trend is observed. It may be attributed to homogeneous flow regime. However, results for other system have to be examined.

For air/ethylene glycol solution system the bubble column was operated at much higher values of U_g. Value of σ for this system as a function of U_g, H_s and Z= 0.15 m are presented in Figure (4.30). It is observed that standard deviation increases with increasing value of U_g and H_s. However, the value of σ is did not depend upon the concentration of ethylene glycol.

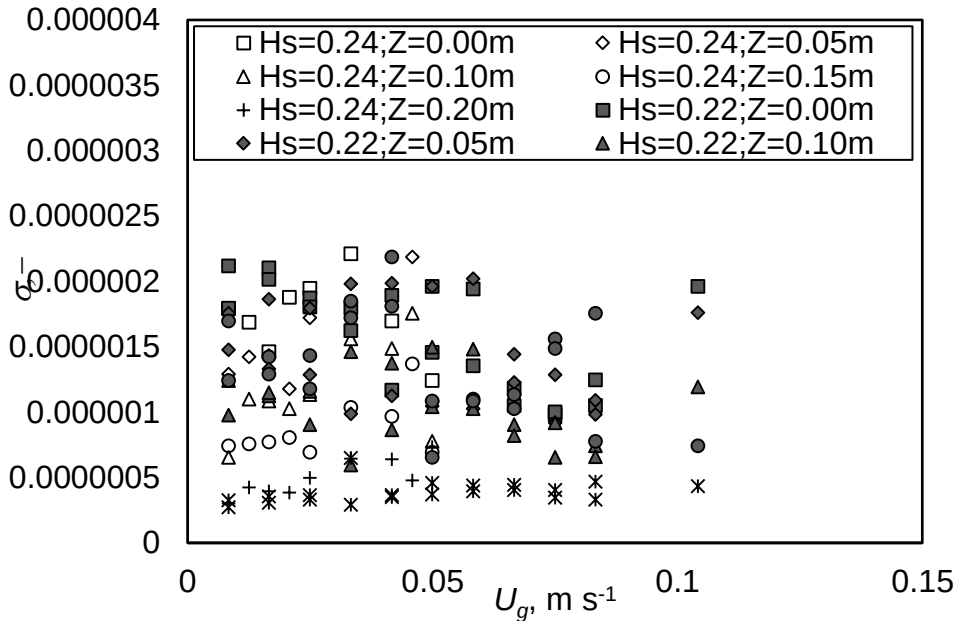

Figure 4.28: Value of σ for air-water system as a function of U_g, H_s, Z=0.15 m.

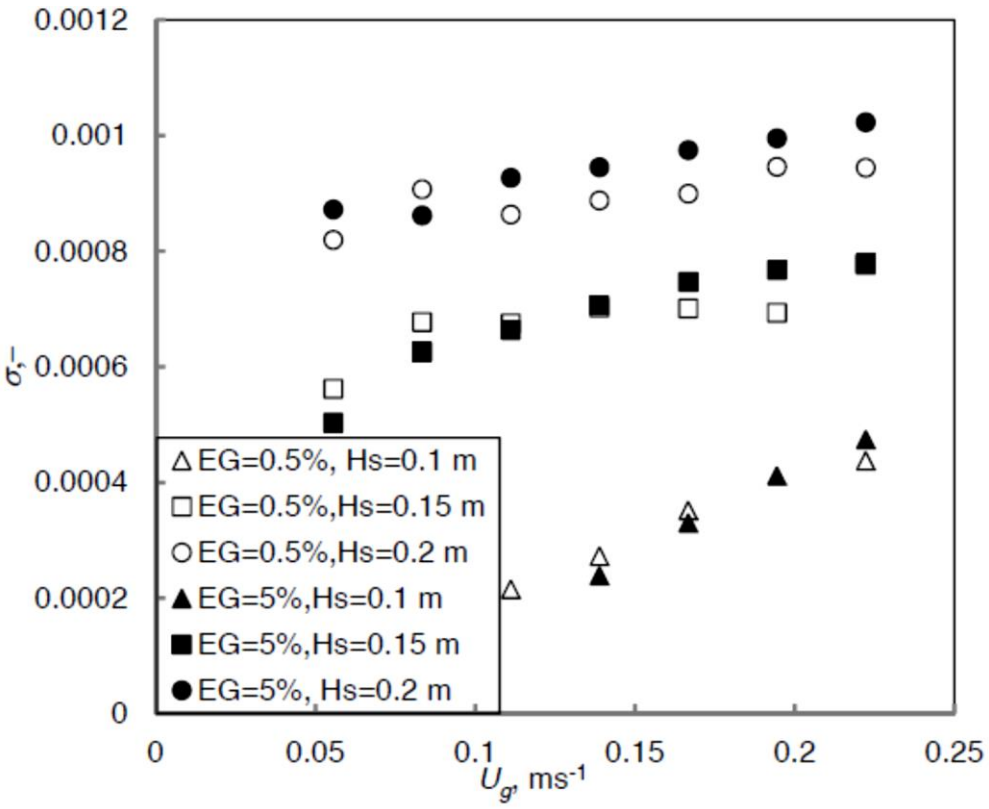

Figure 4.29: Value of σ for air-EG soln. system as a function of U_g, H_s, Z=0.15 m.

The values of s_1 and k_1 for air/ethylene glycol solution system as a function of U_g, H_s and Z= 0.15 m are presented are presented in Figures (4.30) and (4.31) respectively. In both cases no definite trend was observed. The values of k_1 was surprisingly constant all values of U_g and H_s. It may be noted that all these values are 0.15 m above the distributor plate and the bubbles had sufficient time for coalescence and break-up.

Due to insensitivity of s_1 and k_1 for air/ethylene glycol solution system towards operating parameters, the values for other systems are not presented. Only the values for standard deviation for other systems are presented.

For air/NaOH solution value of σ for this system as a function of U_g, H_s and Z= 0.05 m are presented in Figure (4.32). The standard deviation at low values of U_g

shows a large scatter. As the value as U_g increases, the scatter reduces drastically, indicating a change in flow regime. No define dependence on NaOH concentration and H_s are observed.

For air/CMC solution value of σ for this system as a function of U_g, H_s and Z= 0.05 m are presented in Figure (4.33). The standard deviation at low values of U_g shows a large scatter. As the values as U_g increases, the scatter reduces slightly. It may be an indication of change in flow regime, which is expected at high value of U_g. No define dependence on CMC concentration and H_s were observed.

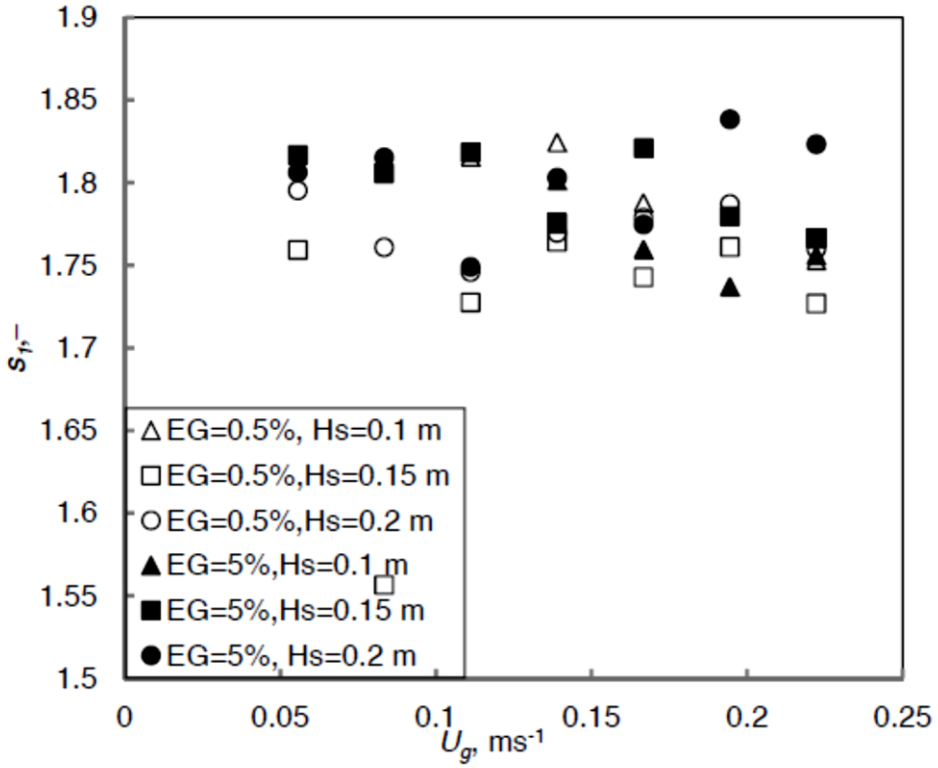

Figure 4.30: Value of s_1 for air-EG soln. system as a function of U_g, H_s, Z=0.15 m.

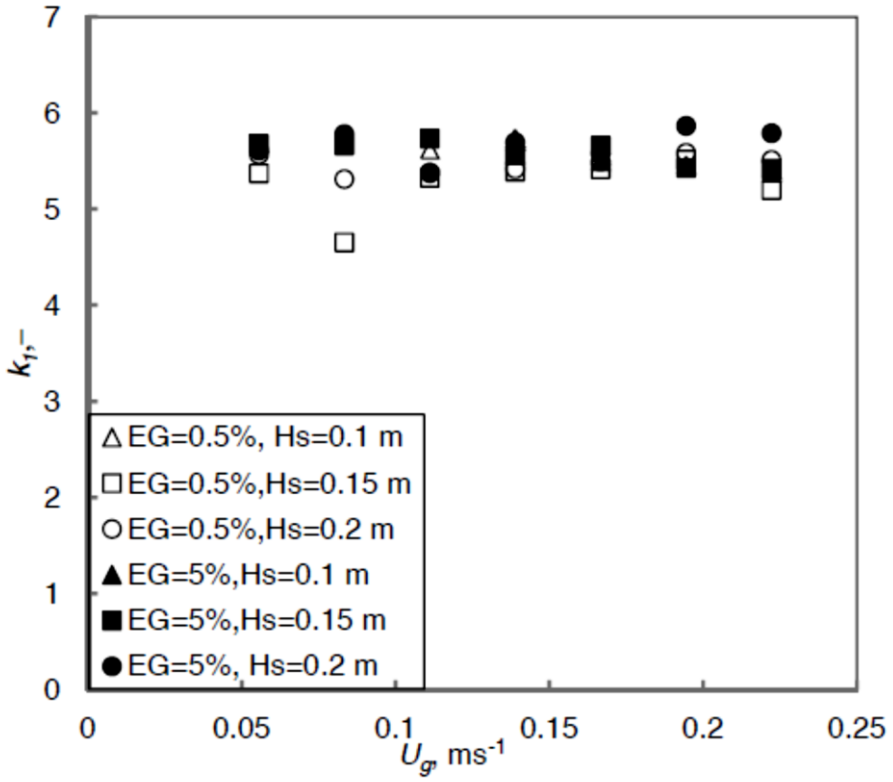

Figure 4.31: Value of k_1 for air-EG soln. as a function of U_g, H_s, Z=0.15 m.

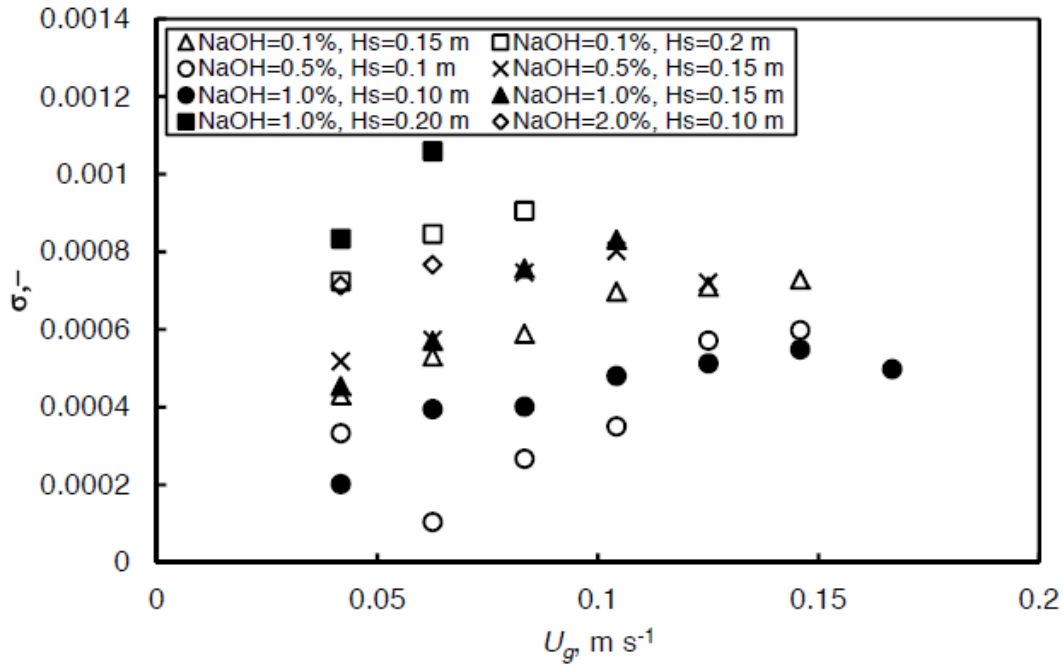

Figure 4.32: Value of σ for air-NaOH soln. as a function of U_g, H_s, Z=0.15 m.

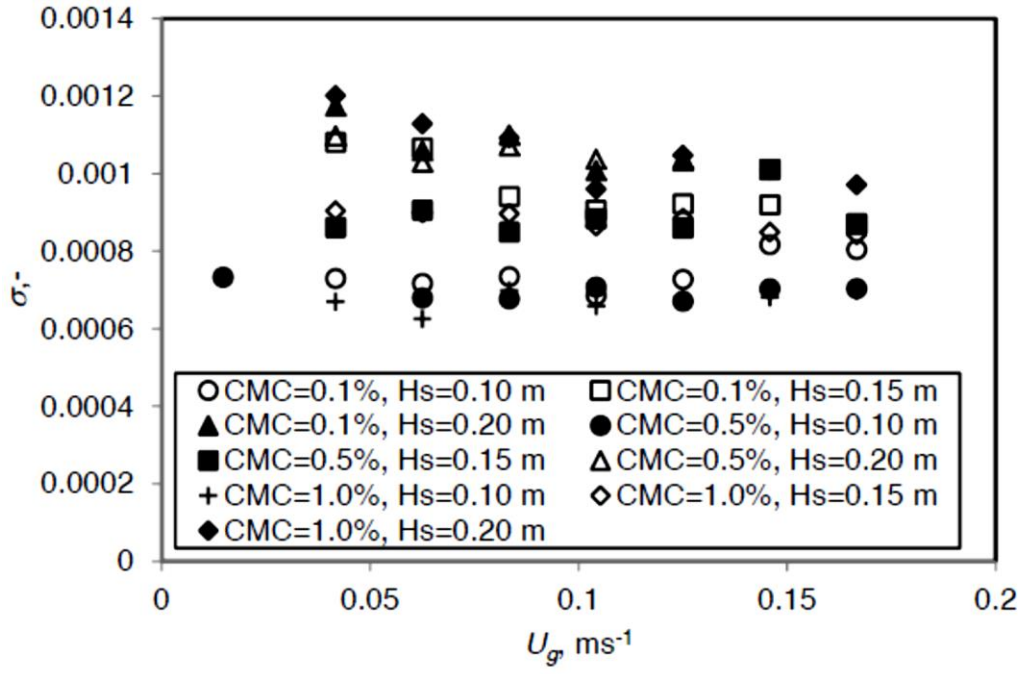

Figure 4.33: Value of σ for air-CMC soln. as a function of U_g, H_s, Z=0.05 m.

4.5 Sauter-mean bubble diameter:

Sauter-mean bubble diameter, d_{32} was calculated by Equation (3.4). Estimation from BSD is also possible, though the values may differ slightly. Estimated values of d_{32} presented in appendix-II.

4.5.1 Effect of H_s on d_{32}:

Variation of d_{32} as a function of U_g for H_s = 0.2, 0.22 and 0.24 m and height above the distributor plate, Z = 0.1 m is presented in Figure (4.34). The values of d_{32} seem to be independent of H_s. Due to small size of the bubble column all values of H_s may be considered as close to each other. Sauter mean diameter does not change if the superficial gas velocity changes. It indicates that there is no change in the flow regime. The observation is in accordance to the finding of BSD, which also showed only one peak for air-distilled water system.

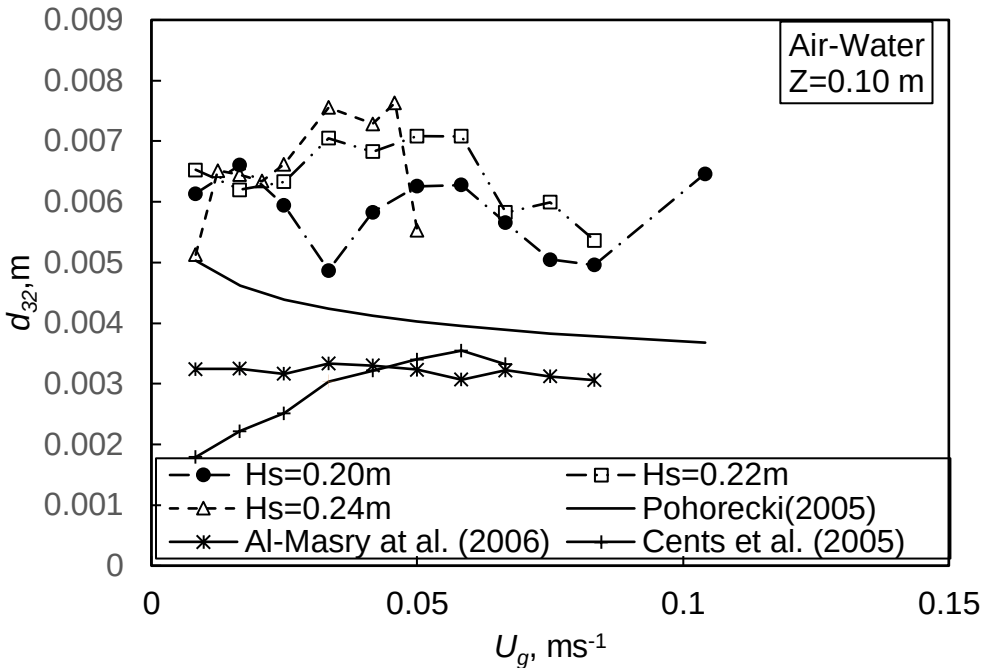

Figure 4.34: Effect of U_g and H_s on d_{32} for air-water system at Z=0.10 m.

Predicted values of d_{32} estimated by Equation (2.8) are also plotted in Figure (4.35). The predicted values of d_{32} decrease with increasing U_g. The experimental values of d_{32} are higher than the experimental values by about 20% at low gas velocity and by about 50% at high gas velocity. Experimental data for tap water measured by Al-Masry et al. [2006] are also shown in the figure. These values are lower than the present values. It may be due to the fact that the hole diameter in their study was 0.001 m. In absence of bubble coalescence and bubble breakup the bubble diameter in the column will be close to that formed at the distributor. The data reported by Cents et al. [2005] for air-water system with sintered sparger are low at low gas velocity. The value of d_{32} decreases with increasing U_g. Other correlations for d_{32} reported in literature require hole-diameter as one of the parameters. The gas distributor in the present work is a combination of glass beads and SS mesh, hole-diameter is not defined. As a result other correlations could not be used for comparison.

4.5.2 Effect of Z on d_{32}:

Variation of d_{32} as a function of U_g for H_s = 0.24 m and height above the distributor plate, Z = 0.0, 0.05, 0.1, 0.15, 0.2 m is presented in Figure (4.35). As the distance above distributor plate, Z, increases from 0.0 m to 0.2 m, the values of d_{32} decreases from 0.008 m to 0.004 m. It is possible in two conditions (i) either there is a bubble break up resulting in gradual decrease of d_{32} with increasing Z or (ii) the smaller bubbles circulate in the column as they are carried away along strong induced current by large bubbles. As a result, the small bubbles are more in upper portion of the column. Bubble breakup is less probable as it was not observed visually. The values of d_{32} are independent of U_g except the values at the distributor plate (Z = 0.0 m). Values of d_{32} estimated using Equation (3.4) are also shown in Figure (4.36). These are in close agreement with those at Z = 0.2 m. The present values of d_{32} are higher than that reported by Al-Masry et al. (2005) and Cents et al. (2005).

In literature contrary conclusions have been reported. Pohorecki et al. (1999) observed that value of d_{32} is constant. In a later work Pohorecki et al. (2005) observed that d_{32} decreases with increasing U_g. Similar results have been reported by Millies and Mewas (1999) and Akita and Yoshida (1974).

The decreasing values of d_{32} with increasing value of Z (distance above distributor plate) is in contradiction to the findings of Schäfer et al. (2002) who observed that the value of d_{32} increased as the bubbles moved up away from the distributor plate. It indicates that bubble break-up dominates in the present study while bubble coalescence was dominant in the studies of Schäfer et al. (2002).

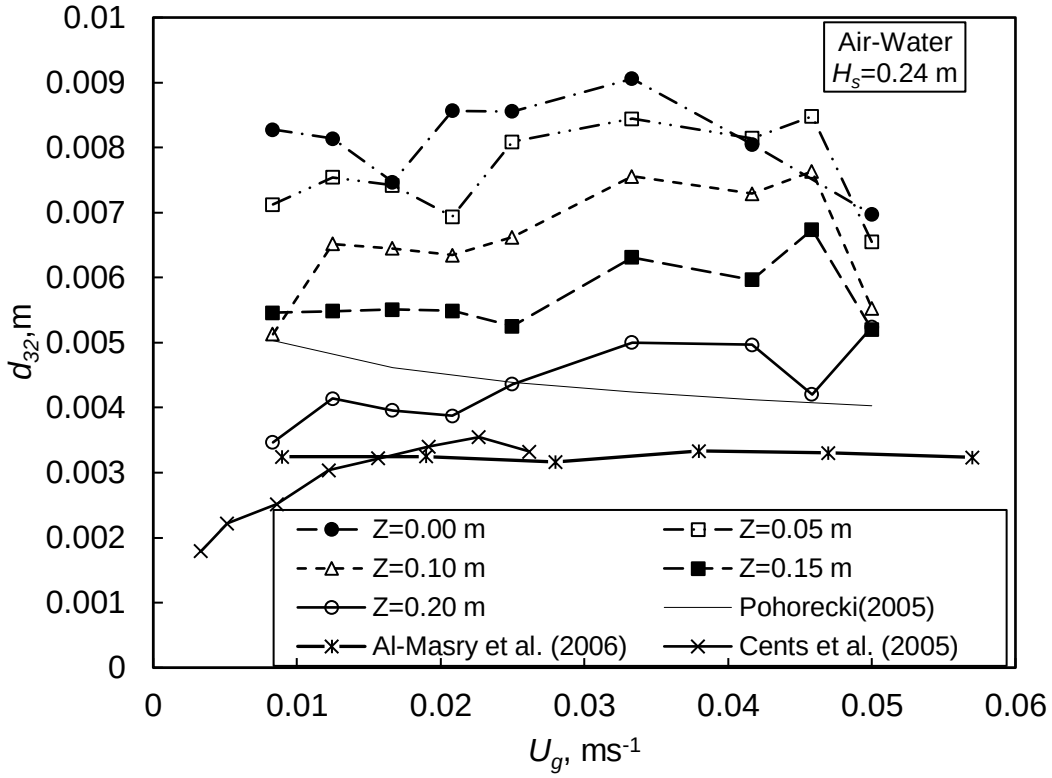

Figure 4.35: Effect of U_g and Z on d_{32} for air-water system at H_s =0.24 m.

4.5.3 Air-Ethylene Glycol soln. System:

Variation of d_{32} as a function of U_g for H_s = 0.20 m and conc. (w/w) of EG= 0.5% and 5.0 %, and Z =0.00 m, 0.05 m and 0.015 m is presented in Figure (4.36). For comparison purpose the values of air-distilled water, hereafter referred as water, are also shown. The values of d_{32} seem to be independent of U_g indicating no change in the flow regime. Though the values of d_{32} are higher than that for air-water system, the concentration of EG shows no significant effect on d_{32}. As the values of Z increases, the values of d_{32} decreases i.e. the bubble size decreases after the bubbles leave the sparger. Equation (3.4) shows that d_{32} to decrease with increasing U_g. It is in accordance with earlier findings of Pohorecki et al. (1999).The experimental values of d_{32} are independent of U_g. Since EG solution has density and viscosity higher than that of

water and has surface tension lower than that of water, the vales of d_{32} estimated using Eqn. 3 for EG solution must be lower than that of water. However, the present experimental values of d_{32} are higher than that of water. Examining the values of d_{32} at the sparger (Z=0.00 m) it can be observed that bubbles formed at the sparger in the case of EG solutions are larger than that formed in case of water.

4.5.3.1 Effect of Z on d_{32}:

As the value of Z, increases from 0.00 m to 0.15 m, the values of d_{32} decreases by 40% in case of water as well as in case of EG solution. It may be possible only when either bubble breakup is more prominent than bubble coalescence or small bubbles in the column are carried away towards the top along strong induced current by large bubbles resulting in accumulation of small bubbles in the upper portion of the column. Bubble breakup is less probable as it was not observed visually. Present trend is in contradiction to the findings of Schäfer et al. (2002) who observed that the value of d_{32} increased as the bubbles moved up away from the distributor plate possibly due to bubble coalescence being dominant in their studies.

4.5.3.2 Effect of H_s on d_{32}:

Variation of d_{32} for 5.0% (w/w) aq. soln. of EG as a function of U_g for H_s = 0.10, 0.15 and 0.20 m and Z = 0.05 m is presented in Figure (4.37). The value of d_{32} increases with increasing value of H_s, which could be due to more residence time available for bubbles to coalescence. This trend is surprising as for the same vale of H_s value of d_{32} decreases with increasing value of Z.

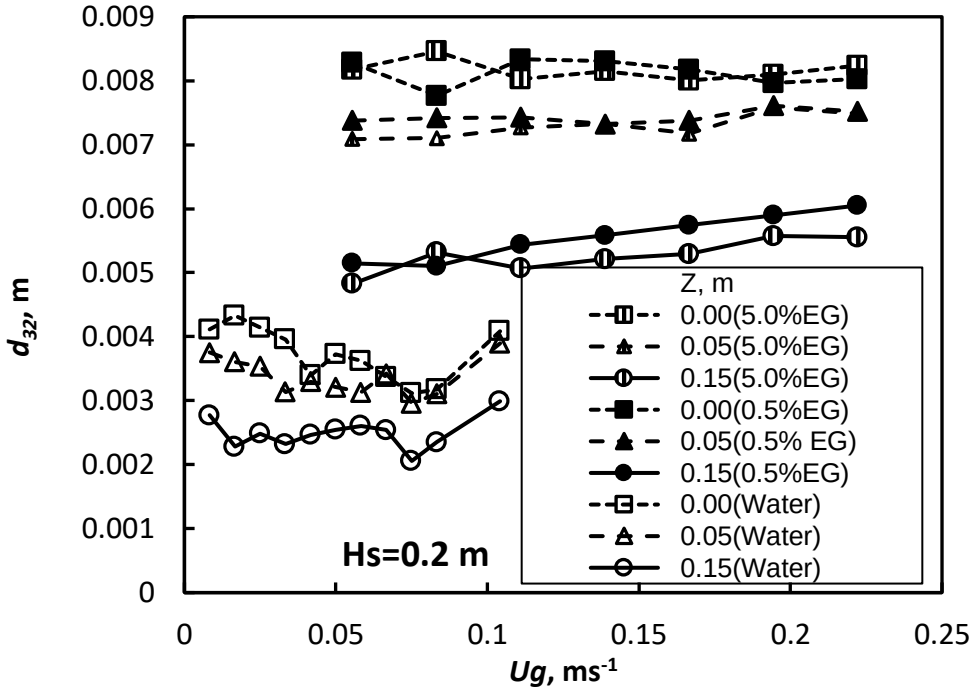

Figure 4.36: Sauter-mean diameter as a function of U_g and Z for air-water and air-ethylene glycol solutions.

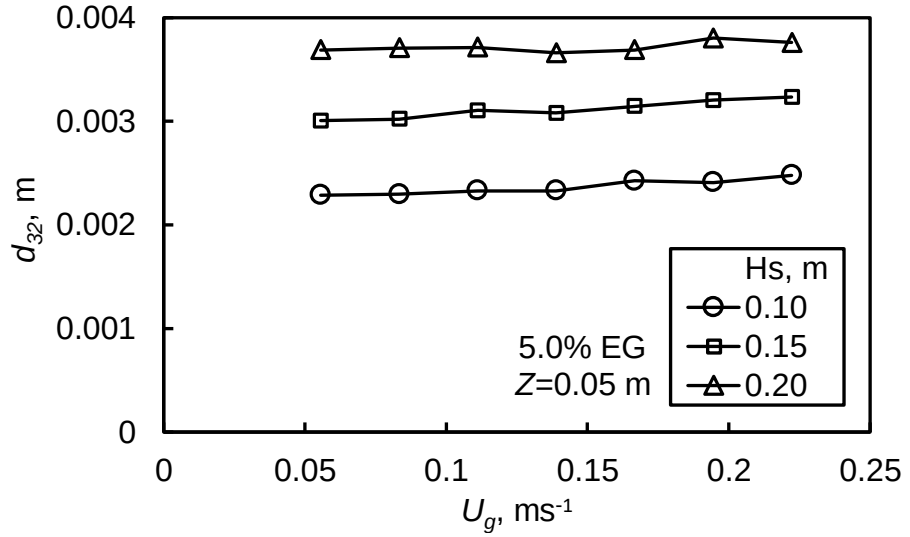

Fig. 4.37: Effect of H_s and U_g on d_{32} for 5% (w/w) ethylene glycol solution at Z=0.05 m.

4.5.4 Sauter-Mean Bubble Diameter for Air/aq. CMC Soln.:

Due to foam forming tendency the experiments were performed at H_s = 0.10, 0.15 and 0.20 m. As a result at low value of H_s the mikes at position Z=0.20 m was not completely submerged in the solution. The data in such cases could not be taken.

4.5.4.1 Effect of H_s on d_{32}:

Variation of d_{32} for 0.1% (w/w) aqueous solution of CMC as a function of U_g for H_s = 0.10, 0.15 and 0.20 m and height above the distributor plate, Z = 0.0.05 m is presented in Figure (4.38) The value of d_{32} increases with increasing value of H_s, which could be due to more residence time available for bubbles to coalescence. BSD also shows that maximum bubble diameter increased with increasing Z. The value of d_{32} is independent U_g.

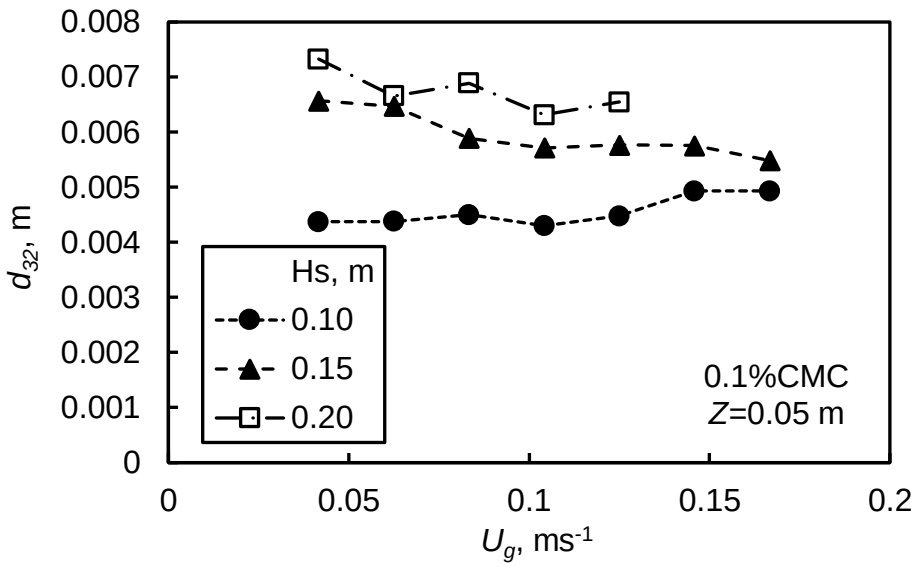

Figure 4.38: Effect of U_g and H_s on d_{32} for air-aq. CMC soln. at Z=0.10 m.

4.5.4.2 Effect of Z on d_{32}:

Variation of d_{32} for 0.1% (w/w) aqueous solution of CMC as a function of U_g and Z for H_s = 0.15 m is presented in Figure (4.39). The value of d_{32} decreases with increasing value of Z. It may be attributed to bubble breakup. The trend is in accordance with that observed in Figure (4.38), which shows that as H_s increases, d_{32} decreases. The BSD shows the reduction of maximum bubble diameter with increasing value of Z. However, the increasing d_{32} with increasing Z is due to large number of intermediate sized bubbles at large distance above the distributor. From trends of BSD and d_{32} it may be said that bubble coalescence and bubble breakup takes place in the column and hence the flow regime is churn-turbulent.

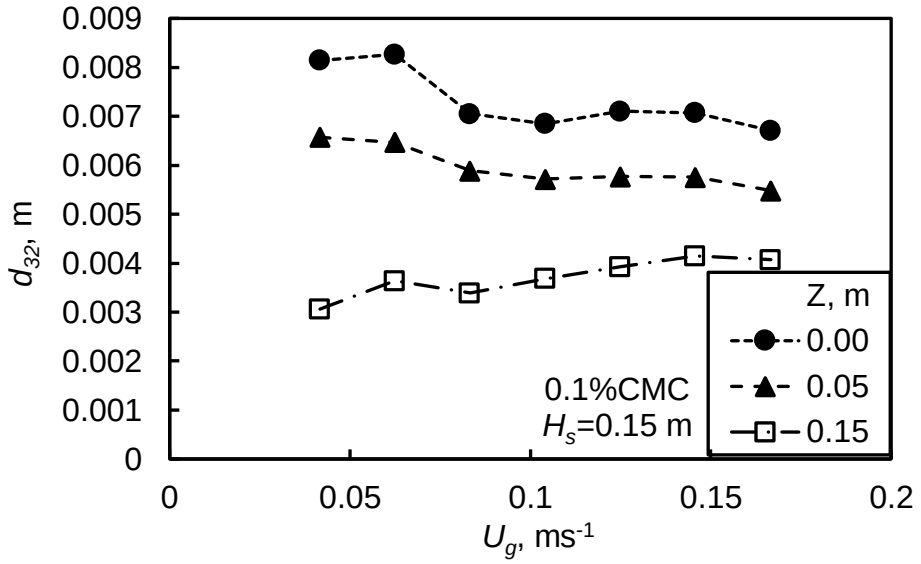

Figure 4.39: Effect of U_g and Z on d_{32} for air-0.1% (w/w) CMC soln. at H_s=0.15 m.

4.5.4.3 Effect of Concentration of CMC on d_{32}:

Variation of d_{32} for 0.1% (w/w) aqueous solution of CMC as a function of U_g and Z for H_s = 0.15 m is presented in Figure (40). The value of d_{32} is independent of CMC concentration. The value of d_{32} is about 100% higher than that in case of air-water system. Al-Masry et al. (2007) reported that at high concentration of CMC the values of d_{32} are low. The present observation is not in accordance with their data. Jamialahmadi et al. (2001) reviewed effect of viscosity on size of bubble during its formation and pointed out that as the liquid viscosity increases, the size of the bubble decreases. Therefore, it seems that the contradiction is due to the fact that it is not bubble formation but bubble coalescence and bubble breakup phenomena dominates the bubble behavior.

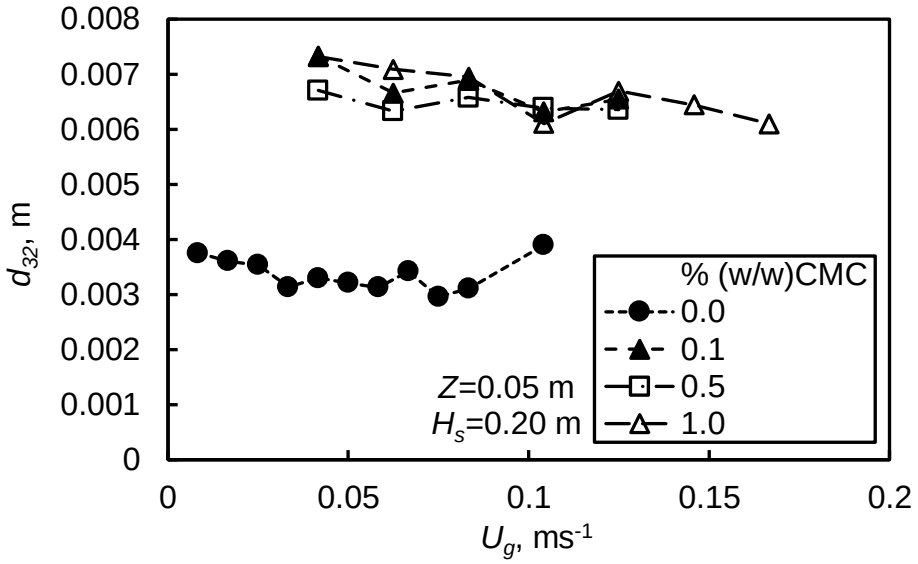

Figure 4.40: Effect of CMC conc. on d_{32} at H_s=0.20 m and Z=0.05 m.

Thus, values of d_{32} measured using acoustic method in the present study are comparable with the values reported in literature. Its variation with height above the distributor illustrates that the technique can be used to find out if there is any bubble-coalescence in the column.

4.5.5 Air-NaOH soln. system:

4.5.5.1 Effect of *Z:*

Variation of d_{32} with U_g for 0.1%(w/w) NaOH soln. at H_s =0.10 m and Z=0.00, 0.05 and 0.15 m is presented in Figure (4.41). Near the sparger i.e. at Z=0.00 and 0.05 m, d_{32} is independent of U_g. But at Z=0.15 m d_{32} increases with increasing U_g. It is clear indication that as the bubble moves in the column, bubble breakup takes place. Visually, NaOH exhibited foam formation.

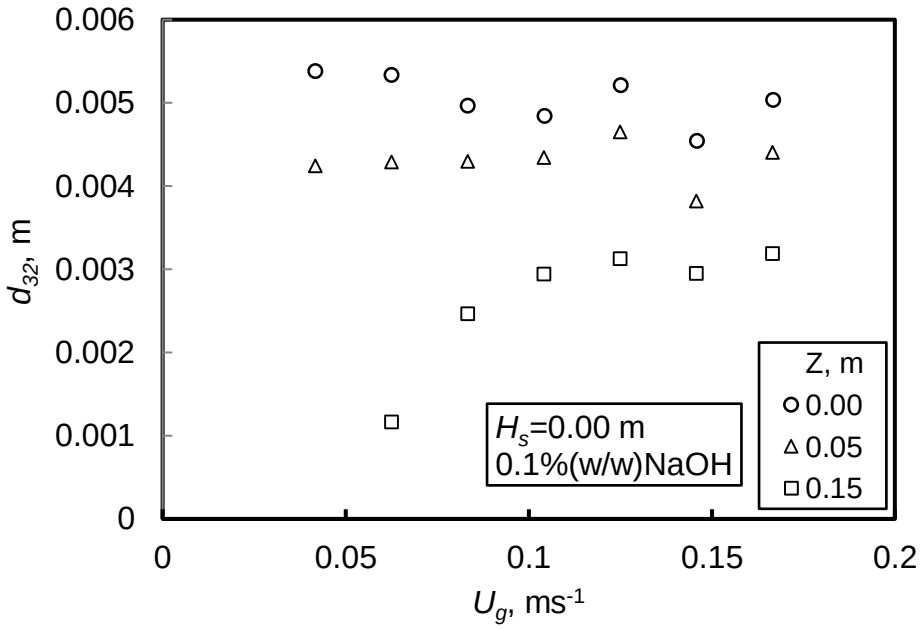

Figure 4.41: Variation of d_{32} with U_g and Z for 0.1% (w/w) NaOH soln. at H_s =0.10 m.

4.5.5.2 Effect of H_s:

Values of d_{32} with U_g for 0.1%(w/w) NaOH soln. at H_s =0.10, 0.15 and 0.20 m and Z=0.05 m is presented in Figure (4.42). Values of d_{32} are independent of U_g. At H_s = 0.2 m the values of d_{32} is about 30 to 40 % higher than that at H_s = 0.1 m and 0.15 m.

4.5.5.3 Effect of NaOH conc.:

Effect of concentration of NaOH on values of d_{32} with U_g at H_s =0.15 and Z=0.05 m is presented in Figure (4.43). While at NaOH con. =0.1 and 1.0 %(w/w) value of d_{32} increases with increasing U_g, value of d_{32} at NaOH con. =0.5 %(w/w) shows reverse trend. This behaviour could not be understood. Certainly concentration of NaOH plays a role in affecting d_{32} in two diffenernt ways.

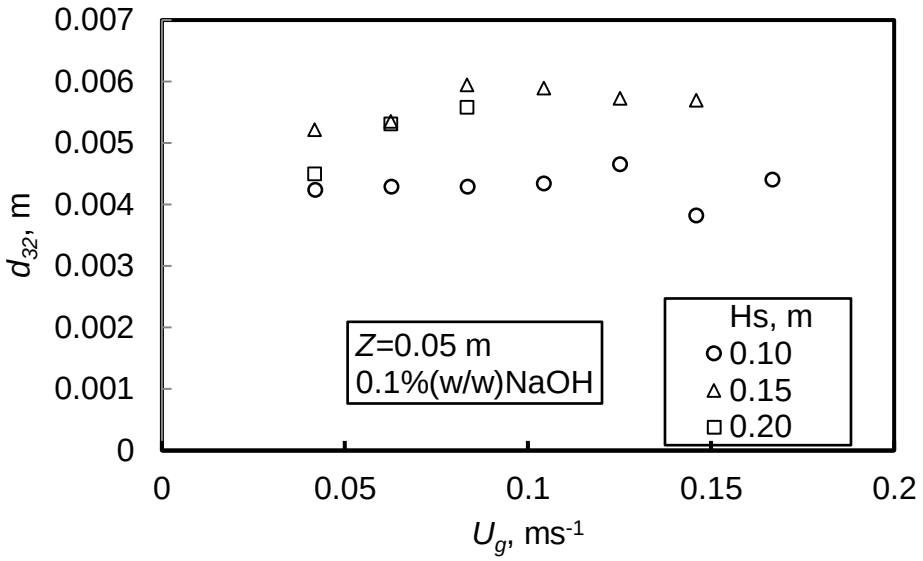

Figure 4.42: Variation of d_{32} with U_g and H_s for 0.1% (w/w) NaOH soln. at Z =0.05 m.

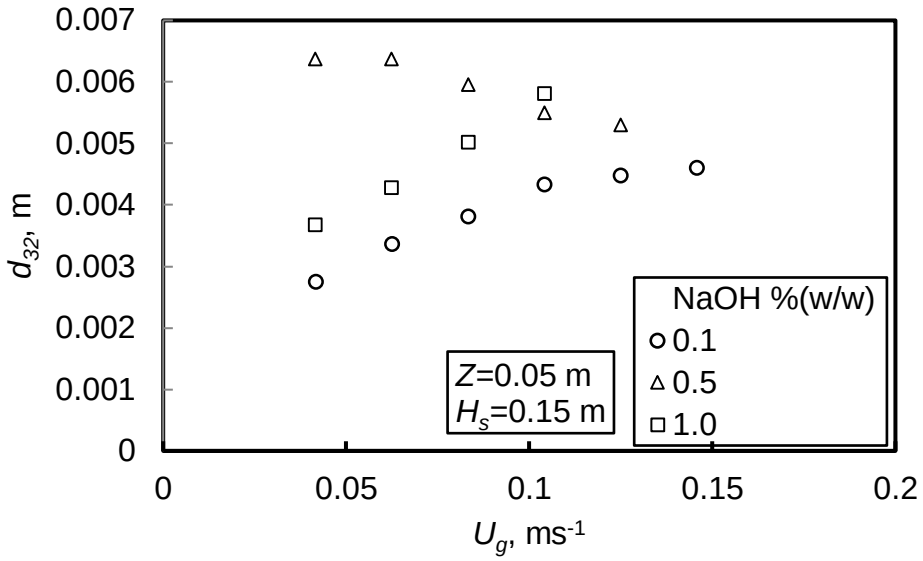

Figure 4.43: Variation of d_{32} with U_g for 0.1% (w/w) NaOH soln. at Z =0.05 m and H_s =0.15 m.

4.6 Gas holdup

Gas holdup is required for the estimation of specific interfacial area. It was experimentally determined from the values of expanded bed height, H_e.

$$\varepsilon = (H_e - H_s)/H_e \qquad (4.5)$$

The entire data is presented in appendix-II. Values of ε at H_s= 0.20, 0.22 and 0.24 m for air-water and H_s = 0.10, 0.15 and 0.20 m for aqueous solutions CMC=0.1, 0.5 and 1.0 wt. % were presented in Figure (4.44). Gas goldup increases with increasing U_g. No specific trend on effect of concentration of CMC and H_s on gas holdup could be observed. The static bed height of CMC solutions should be kept low so that the mikes are always submerged in the solution to provide acoustic signals.

Values of ε at H_s= 0.10 m , 0.15 m and 0.20 m for air-aq. EG soln. and H_s= 0.20 m for air-water are presented in Figure (4.45). Gas goldup increases with increasing U_g. Its values for aq. soln. of EG are lower than that for water. Dues to

higher gas holdup, the data could not be obtained for high value of U_g to avoid overflow. No specific trend on effect of conc. of EG and H_s on gas holdup were observed. It was essential keep the mikes always submerged in the solution.

Gas holdup data were obtained so that it could be used to estimate values of a_i and was not the aim of this study. Hence, the data of ε for other systems is not discussed.

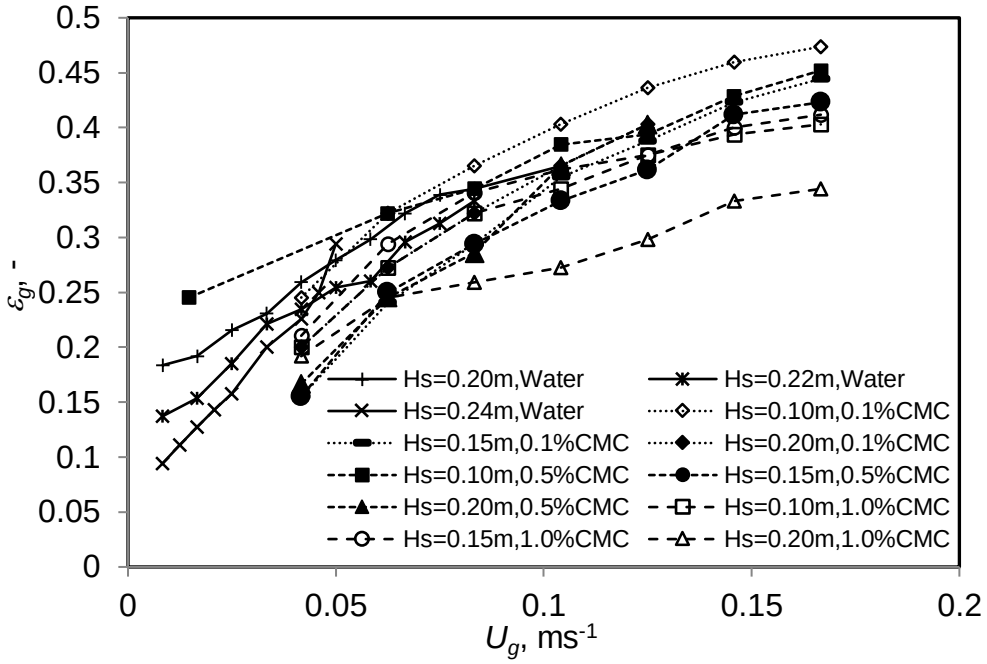

Figure 4.44: Gas holdup as a function of U_g and H_s for air-water and air-CMC solutions.

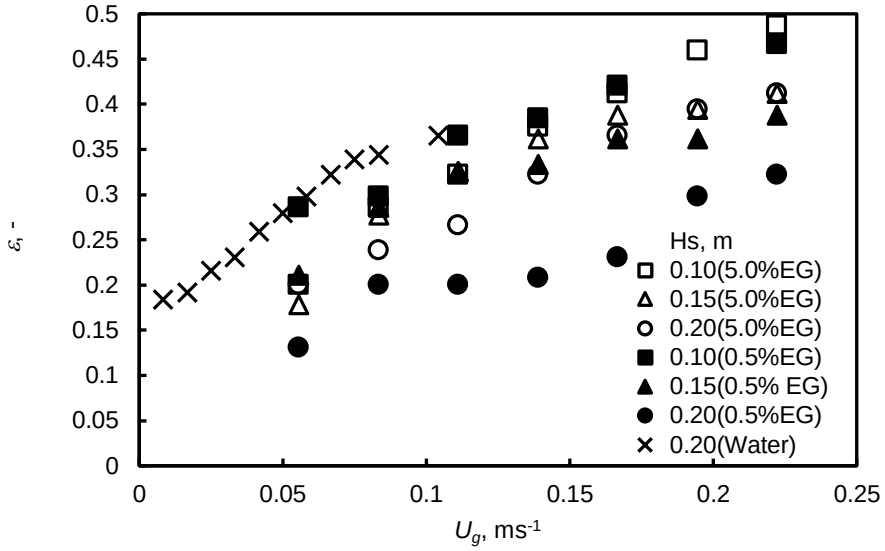

Figure 4.45: Gas holdup as a function of U_g and H_s for air-water and air-ethylene glycol solutions.

4.7 Specific interfacial area, a_i:

Specific interfacial area, a_i were estimated using Equation (2.9). The values are presented in appendix-II. The trends are presented and discussed in this section.

4.7.1 a_i for air-water system:

4.7.1.1 Effect of Z on a_i:

To understand the effect of distance above distributor plate, values of a_i as a function of U_g for mike positions, Z = 0.0, 0.5, 0.1, 0.15 and 0.2 m at H_s = 0.24 m are presented in Figure (4.46). As expected, value of a_i increases with increasing U_g in all the cases. It is due to the fact that high number of bubbles generated at the gas distributor at large gas velocity. The rate of increase of a_i is small for $0.02 < U_g < 0.04$ ms^{-1}. This trend is in accordance with the findings reported in literature [Pohorecki et al. (1999), Schäfer et al. (2002), Bouaifi et al. (2001)]. Values of a_i for Z = 0.00, 0.05 and 0.10 m are close to each other. For $Z > 0.10$ m the value of a_i increases with increasing

Z. It may be attributed to the fact that the mikes were close to the foam layer present in the column. Existence of foam layer was confirmed visually. The variation of a_i with Z is in accordance with the findings of Schäfer et al. (2002). Data of Cents et al. (2005) are in close agreement to the values of a_i for Z=0.15 m and 0.20 m. Estimated values of a_i using correlation of Pohorecki et al. (2005), given in Table 2.4, are plotted in Figure (4.46).. These values are in close agreement to the values of $\underline{a_i}$ at Z= 0.0 m.

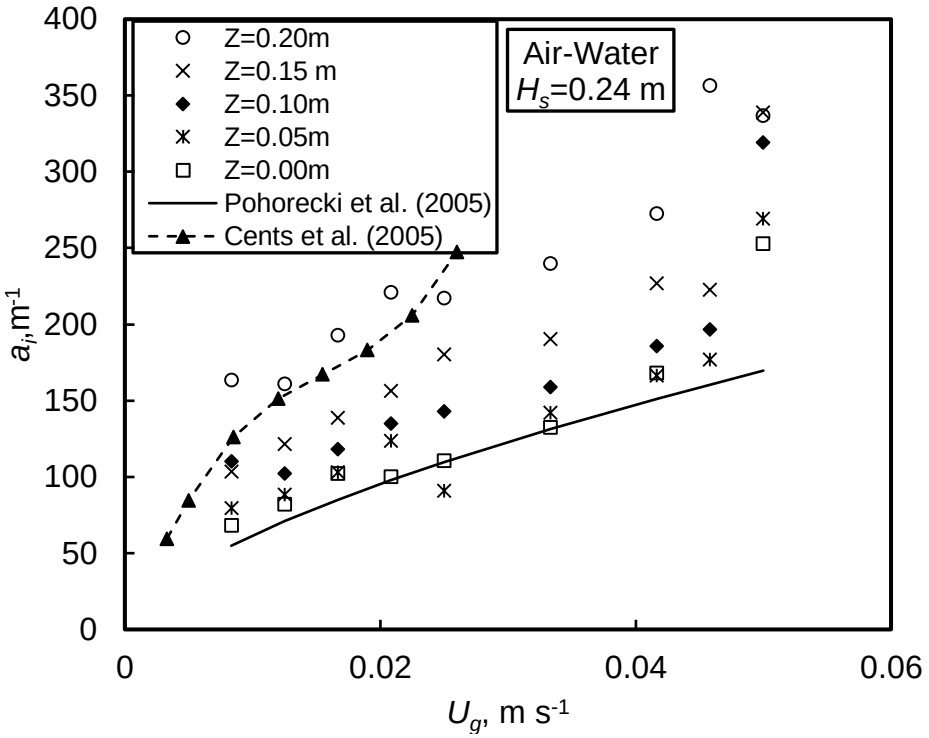

Figure 4.46: Values of a_i for air-water system as a function of U_g and Z at H_s=0.24 m.

4.7.1.2 Effect of H_s on a_i :

Variation of a_i with U_g for static bed height, H_s = 0.2, 0.22 and 0.24 m for Z = 0.15 m is presented in Figure (4.47). Values of a_i increase with increasing U_g and decreasing H_s. The effect of H_s on a_i may be attributed to a combined effect of ε and d_{32}. The value of a_i is almost constant for U_g > 0.08 m s^{-1}. All the values are about 25% higher than that predicted by Equation (2.8). The values are comparable to the values reported by Cents et al. (2005). However, the data of Cents et al. (2005) are more sensitive to U_g than that for present data.

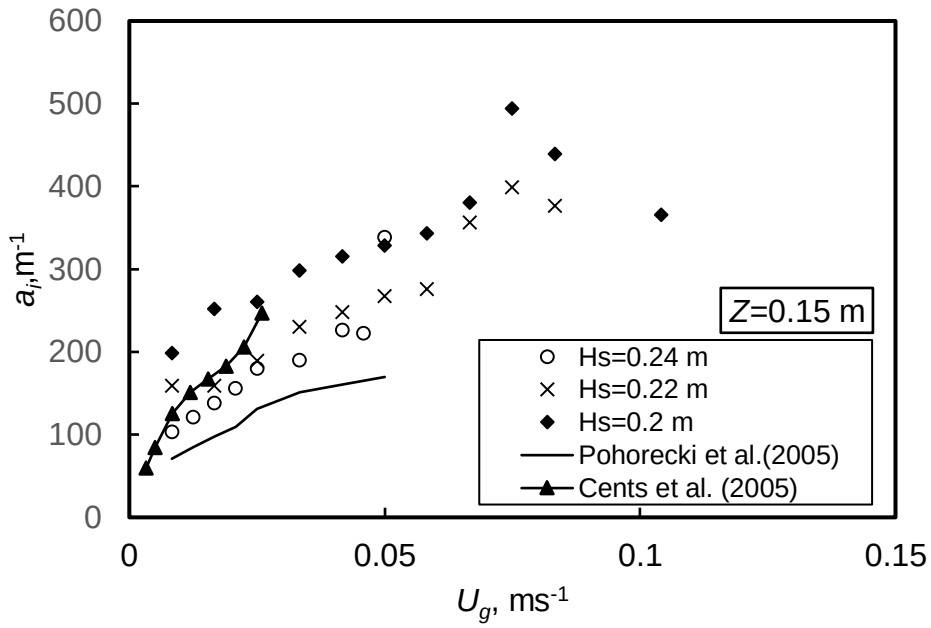

Figure 4.47: Values of a_i for air-water system as a function of U_g and H_s at Z =0.15 m.

4.7.2 Specific Interfacial Area for Air-aq. CMC Soln.:

4.7.2.1 Effect of H_s on a_i:

Variation of a_i for 0.5% (w/w) aqueous solution of CMC as a function of U_g for H_s at Z = 0.05 m is presented in Figure (4.48). Value of a_i increases as the value of H_s decreases. This trend is similar to that observed for air-water system. The value of a_i is inversely proportional to d_{32} and proportional to ε. For air-CMC solution the value of d_{32} increased with increasing H_s. Since d_{32} did not show any significant dependence on H_s, decrease in a_i with increasing H_s is expected.

4.7.2.2 Effect of Z on a_i:

Values of a_i as a function of U_g and Z=0.00, 0.05 and 0.15 m for 0.1% (w/w) CMC solution and H_s= 0.15 m are presented in Figure (4.49). The value of a_i increases with increasing U_g. Since the values of d_{32} were independent of U_g, the increase of values of a_i with increasing U_g is due to increasing ε. The value of d_{32} decreased with increasing Z, which is an indication that bubble breakup is dominating. Increasing value of d_{32} with increasing Z, is expected.

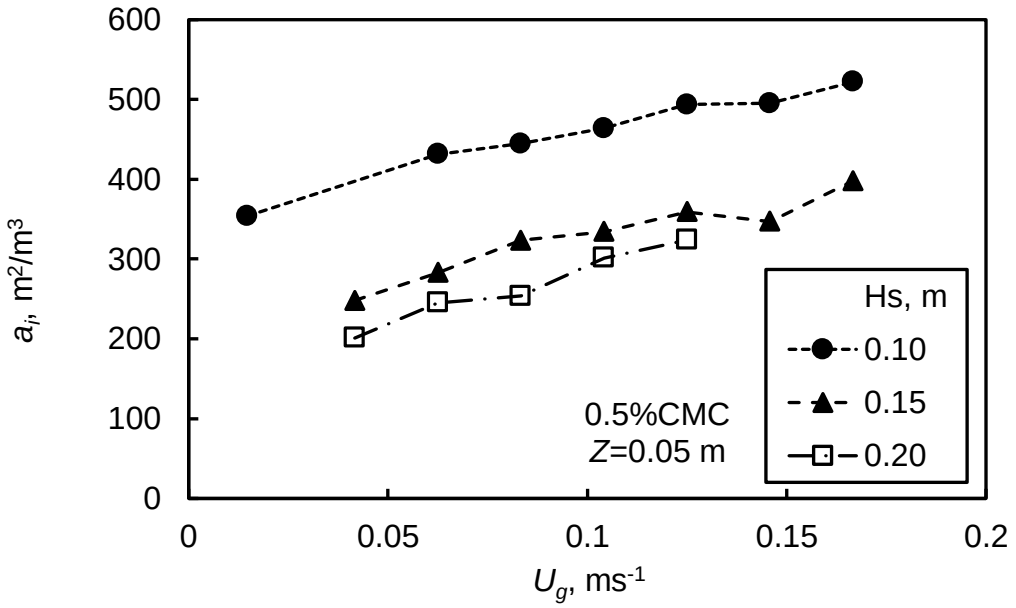

Figure 4.48: Effect of U_g and H_s on a_i for air-0.5 % (w/w) CMC soln. at Z = 0.05 m.

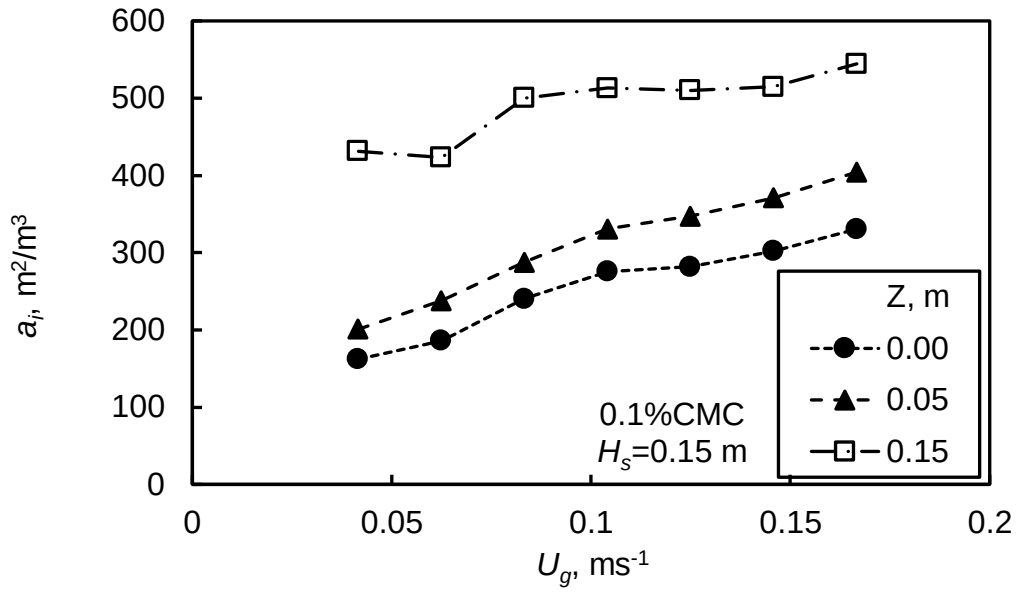

Figure 4.49: Effect of U_g and Z on a_i for air-0.1% (w/w) CMC soln. at H_s=0.15 m.

4.7.2.3 Effect of Concentration on a_i:

Variation of a_i as a function of U_g and concentration of CMC at Z=0.05 m and H_s=0.20 m is presented in Figure (4.50). Values of a_i for air-CMC solution are about 50% lower than that of air-water system. It is in accordance to the trend observed for d_{32}, which, for air-CMC solution, was about 80% higher than that air-water system CMC concentration exhibts very little effect on a_i and is in accordance to the fact that d_{32} also was independent of CMC concentration and the gas holdup did not show any specific dependence on CMC concentration.

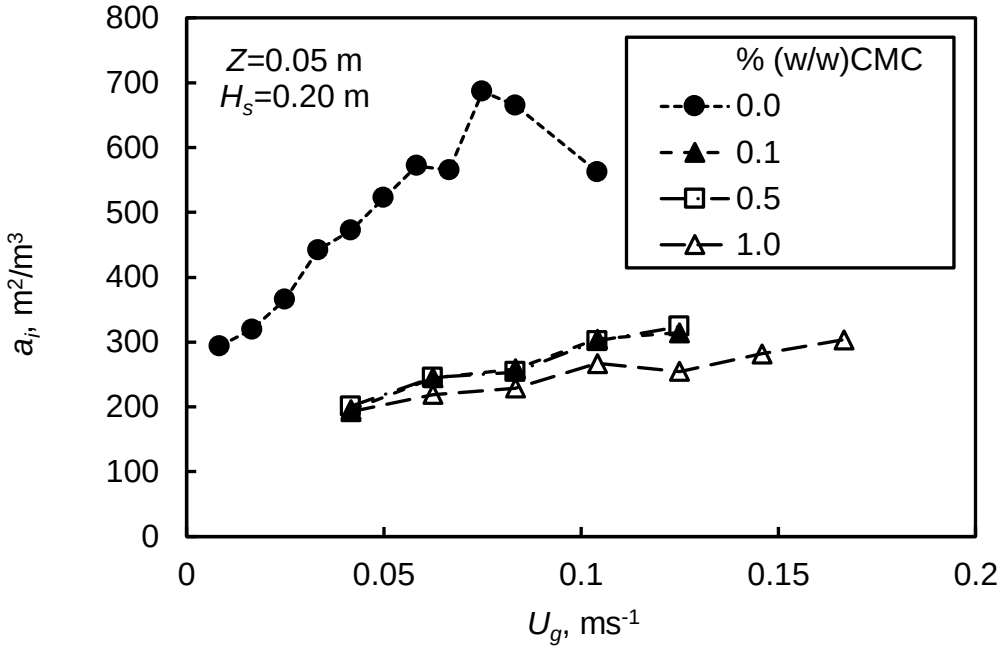

Figure 4.50: Effect of U_g and conc. Of CMC soln. on a_i at Z=0.05 m and H_s=0.20 m.

4.7.3 Specific Interfacial Area for Air/aq. EG Soln.:

4.7.3.1 Effect of U_g and Z on a_i:

Variation of a_i as a function of U_g for H_s = 0.20 m and conc. (w/w) of EG= 0.5% and 5.0 %, and Z =0.00 m, 0.05 m and 0.015 m is presented in Figure (4.51). The value of a_i increases with increasing U_g in all the cases. Since d_{32} is independent of U_g, the increase is due to increase in ε. It is due to the fact that high number of bubbles generated at the gas distributor at large gas velocity. The values of a_i in case of aq. soln. of EG are about 200% lower than that in case of water. No specific dependence on Z could be observed. It might be due to a combined effect of ε and Z. Correlation of Pohorecki et al. (1999) considers only U_g to affect a_i.

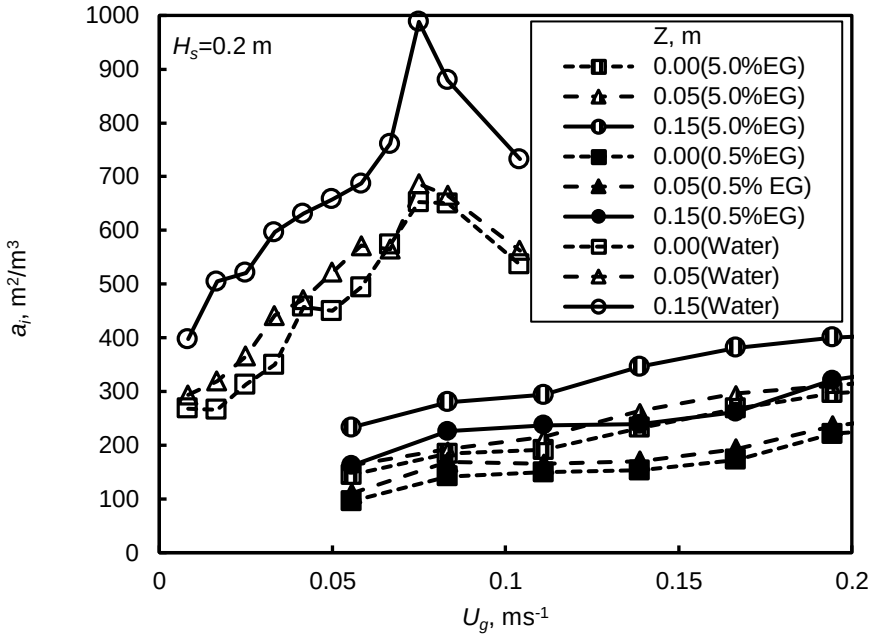

Figure 4.51: Specific interfacial area as a function of U_g and Z for air-water and air-ethylene glycol soln. at H_s = 0.20 m.

4.7.3.2 Effect of H_s on a_i:

Variation of a_i with U_g for static bed height for 5%(w/w) EG soln. at H_s = 0.10 m, 0.15 m and 0.20 m and Z = 0.05 m is presented in Figure (4.52). The value of a_i increases with increasing value of U_g. Since the value of d_{32} is independent of U_g, the trend is due to increasing ε with increasing U_g. The value of a_i increases with decreasing H_s. It may be attributed to decresing value of d_{32} with increasing H_s.

4.7.4 Specific Interfacial Area for Air-aq. NaOH Soln.:

4.7.4.1 Effect of U_g and Z on a_i:

Variation of a_i with U_g for 0.1%(w/w) NaOH soln. at H_s =0.10 m and Z=0.00, 0.05 and 0.15 m is presented in Figure (4.53). Near the sparger i.e. at Z=0.00 and 0.05 m, a_i is independent of U_g. But at Z=0.15 m a_i increases with increasing U_g. The trend is similar to that observed in case of d_{32}.

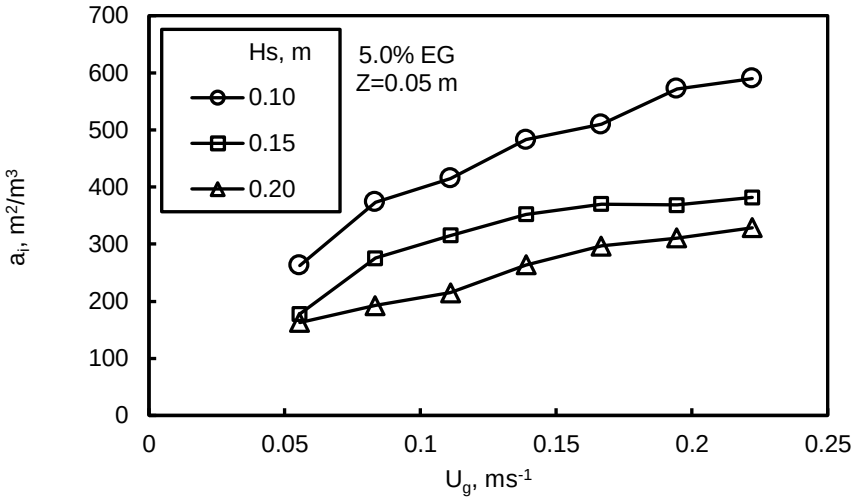

Figure 4.52: Effect of H_s and U_g on a_i for 5% (w/w) NaOH soln. at Z=0.05 m.

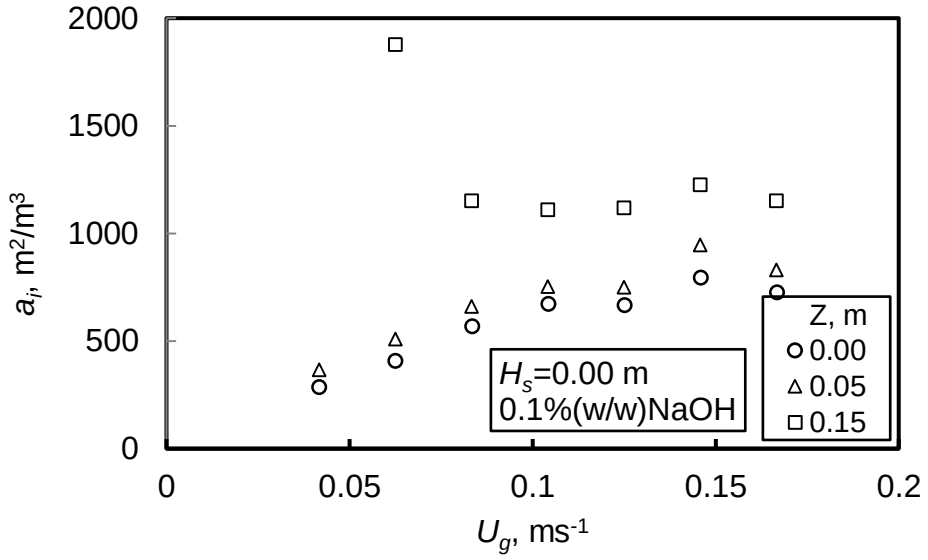

Figure 4.53: Variation of a_i with U_g and Z for 0.1% (w/w) NaOH soln. at H_s =0.10 m.

4.7.4.2 Effect of H_s on a_i:

Variation of a_i with U_g for 0.1%(w/w) NaOH soln. at Z =0.05 m and H_s = 0.10, 0.15 and 0.20 m is presented in Figure (4.54). Value of a_i increases with increasing U_g at all static bed heights. Value of a_i increases with decreasing H_s.

4.7.4.3 Effect of NaOH conc. on a_i:

Variation of a_i with U_g and conc. of NaOH soln. at H_s=0.15 m and Z=0.05 m is presented in Figure (4.55). At NaOH con.=0.1 and 1.0 %(w/w) no effect of concentration is observed. However, at NaOH con.=0.5 %(w/w), the value of a_i at all superficial air velocities are lower than that at other NaOH concentration. The value of a_i increases with increasing U_g. The reasons could not be understood. Similar trend was observed in case of d_{32}.

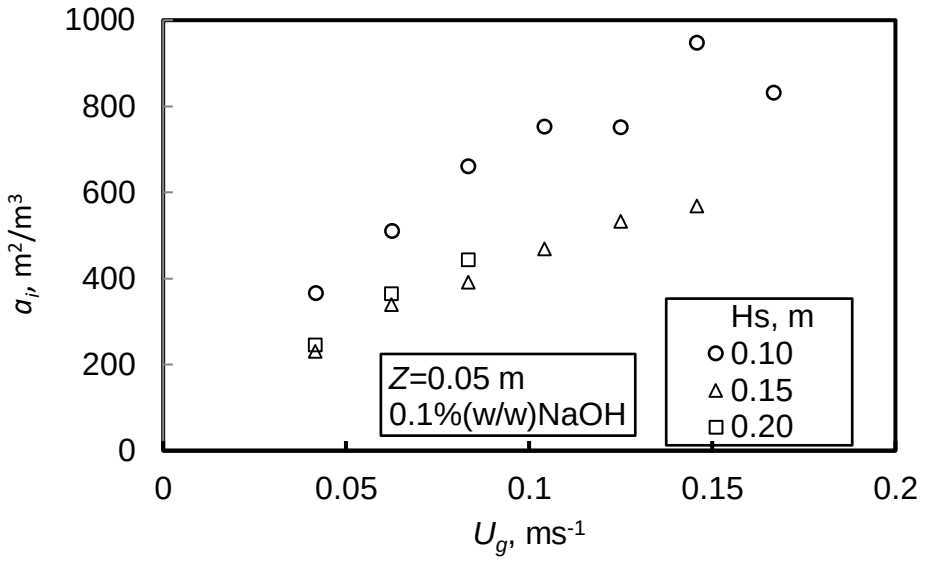

Figure 4.54: Variation of a_i with U_g and H_s for 0.1% (w/w) NaOH soln. at Z =0.05 m.

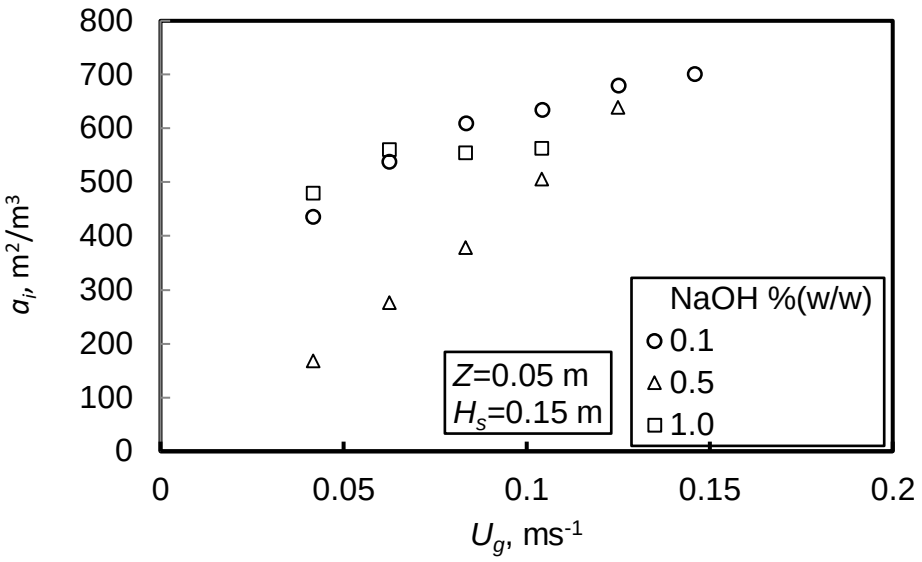

Figure 4.55: Variation of a_i with U_g and conc. of NaOH soln. at Z =0.05 m and H_s =0.15 m.

From the above discussion it is clear that in the present study bubble breakup was dominating. It resulted in reduction of d_{32} as the distance above the distributor increased. Addition of EG resulted in increase of d_{32}. However, since d_{32} increased with increasing Z, it is clear that presence of EG suppressed bubble breakup. It did not enhance bubble coalescence. Addition of CMC and NaOH increased bubble breakup, because the value of d_{32} decreased with increasing Z and concebntration of additives. The nature of the BSD was consistant with these findings. Since, it affects the gas holdup, and depends on gas holdup and d_{32}, the variation of a_i with operating conditions are directly dependent upon d_{32} and ε.

4.8 Mass Transfer Coefficient:

In bubble column, the mass-transfer rate is often measured by oxygen dissolution method. Oxygen or air is bubbled for some time and concentration of

oxygen is measured at different times. Since there is no chemical reaction of oxygen, mass balance of oxygen in the liquid phase can be written as [Moutafchieva et al. (2013)]:

$$\frac{dC}{dt} = k_L a_i \left(C^* - C\right) \tag{4.6}$$

Where C_o is initial concentration of oxygen, C is concentration of oxygen at any time and C^* is concentration of oxygen when the liquid is saturated. Upon integration between t =0 to t, we get

$$k_L a_i t = ln\left(\frac{C^* - C_o}{C^* - C}\right) \tag{4.7}$$

A plot of $ln\left(\frac{C^* - C_o}{C^* - C}\right)$ vs t is a straight line. The value of C^* may be determined by fitting a straight line for a set of data.

Equation (4.7) can also be written as

$$C = C^* - \left(C^* - C_o\right)e^{-k_L a_i t} \tag{4.8}$$

The concentration of O_2 was measured after every 3 minutes with the help of DO meter. All the data were fitted with Equation (4.7) by minimising the SSE as defined below:

$$SSE = \sum\left(C_{exp} - C_{cal}\right)^2 \tag{4.9}$$

Where C_{exp} and C_{cal} are experimental and calculated values of oxygen concentrations. The latter were obtained from Equation (4.8). Since the temperature of the liquid was 20±1^{o}C,the value of C^* was forced to be constant for the entire set of data.

Variation of concentration of oxygen with time for U_g=0.0625 ms^{-1} and H_s=0.10 m is presented in Figure (4.56). It slowly increases with time. The saturation value has not reached even after even after half an hour. The experiment was not carried out for more than half an hour because the amount of water may get reduced due to evaporation resulting in change in concentration of oxygen.

After minimising SSE as defined in Equation (4.9), value of C^* were obtained. A plot of $ln\left(\frac{C^*-C_o}{C^*-C}\right)$ vs t for this data is presented in Figure (4.57). It is straight line passing through the origin. The slope of the line is k_La_i.

Variation of k_La_i with U_g for air-distilled water is presented in Figure (4.58). The data shows a systematic decrease in k_La_i at low gas velocity. The data were repeated few times and same was obtained and could not be explained qualitatively. The concentration measured and used in Equation (4.13) is based on the liquid volume. Therefore, the values of k_La_i are based on the liquid volume. Therefore, the value of k_La_i based on the air-water dispersion is $k_La_i/(1-\varepsilon)$. Variation of $k_La_i/(1-\varepsilon)$ with U_g is also shown in Figure (4.58).

4.9 Model for Mass-Transfer Coefficient:

Mass transfer coefficient based on Higbie's surface renewal model is given by [Verma (2014)].

$$k_L = 1.13\sqrt{\frac{U_{sl}D_{AB}}{d_b}} \qquad (4.10)$$

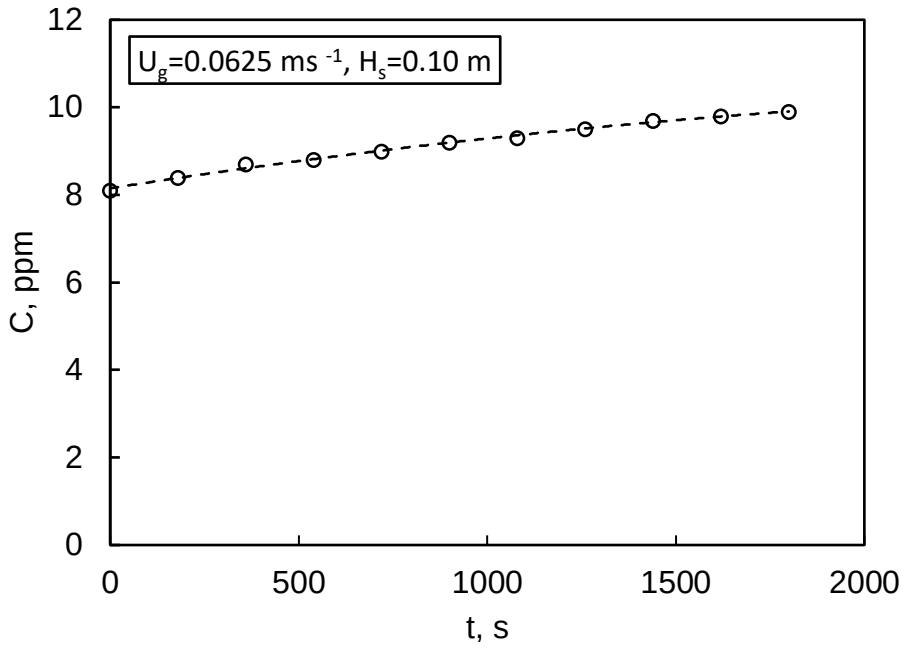

Figure 4.56: Variation of C as a function of time.

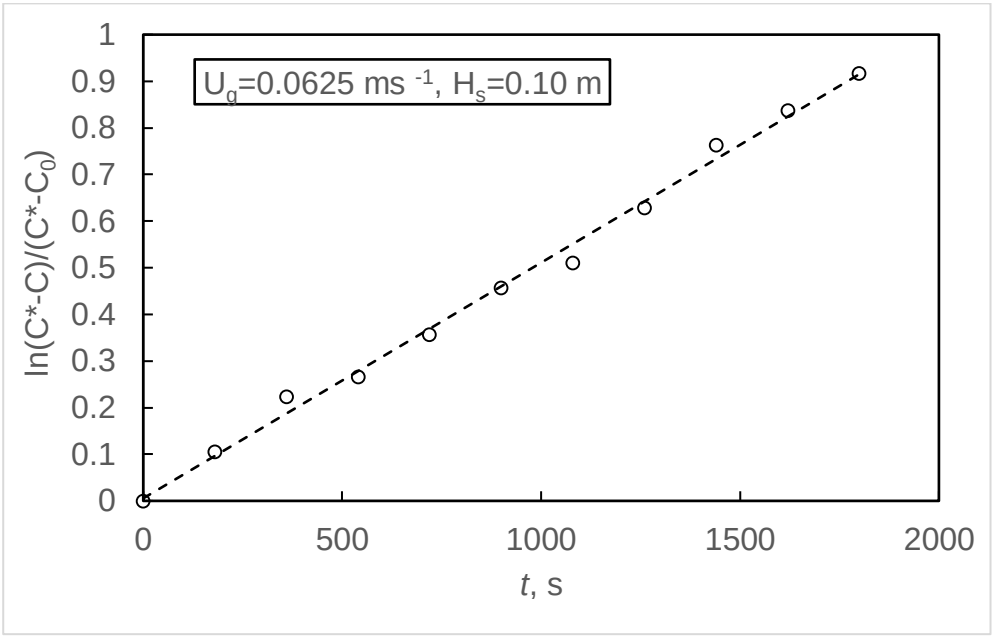

Figure 4.57: Plot of ln(C*-C)/(C*-C_0) vs t.

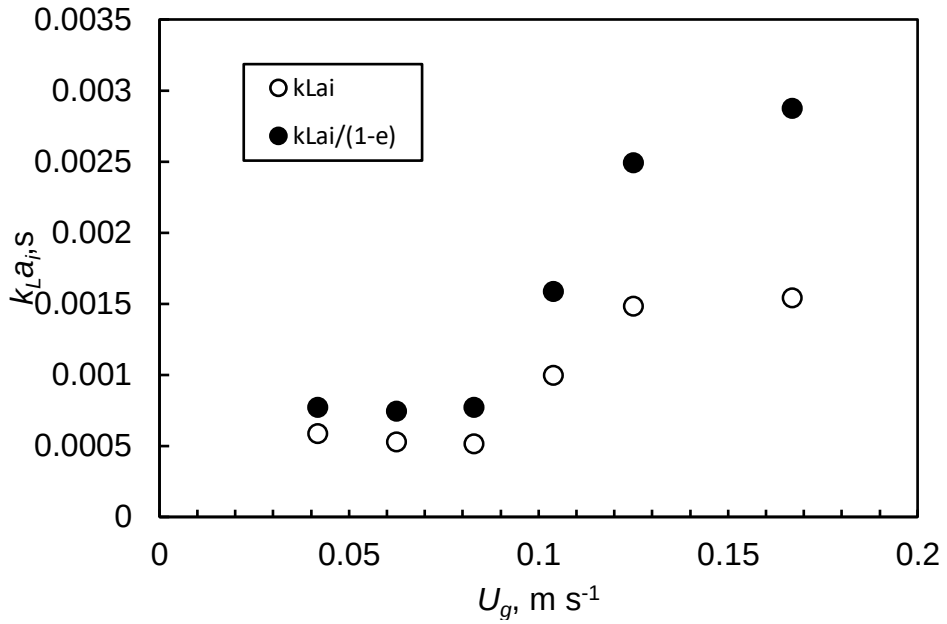

Figure 4.58: Plot of ($k_L a_i$) vs U_g.

Equation (4.10) is valid for surface-to-bulk mass transfer coefficient. To use it for gas-liquid mass-transfer coefficient, U_{sl} should be removed by swarm velocity, V_b. In the present work, it was estimated by following equation [Krishna et al. (1999)].

$$V_b = V_b^0 \left(1-\varepsilon\right)^{n-1} \tag{4.11}$$

For air-water system n=2. The value of V_b^0 is given by

$$V_b^0 = 1.53\left(\sigma g/\rho_L\right)^{0.25} \tag{4.12}$$

Volumetric mass transfer coefficient,($k_L a_i$) can be estimated if the value of d_{32} and a_i are known.

To use the above equation for estimation of k_L for correction for air-water system it was corrected for Schmidt number, Sc. The final equation takes the following form.

$$k_L = 1.13\sqrt{\left(\frac{V_b}{\varepsilon}\right)\frac{D_{AB}}{d_b}}\left(\frac{Sc_{air}}{Sc_{water}}\right)^{0.5} \qquad (4.13)$$

4.10 Estimation of $k_L a_i$

The values of ($k_L a_i$) are estimated as following.

1. Let d_{32}=0.006 m
2. Estimate $a_i = \frac{6\grave{o}}{d_{32}}$ using experimental values of gas holdup.
3. Estimate k_L using Equation (4.13)
4. Estimate ($k_L a_i$) by multiplying the values of k_L and a_i

The estimated values of ($k_L a_i$) are compared with the values of in Figure (4.59). The estimated values of ($k_L a_i$) are within ±20% experimental values at high gas velocity i.e. $U_g \geq 0.1$ m s^{-1}. At low values the estimated values are significantly higher than the experimental values. It was observed that flow regime changes at $U_g \cong 0.1$ m s^{-1}. The model. Therefore is valid only in the churn-turbulent regime.

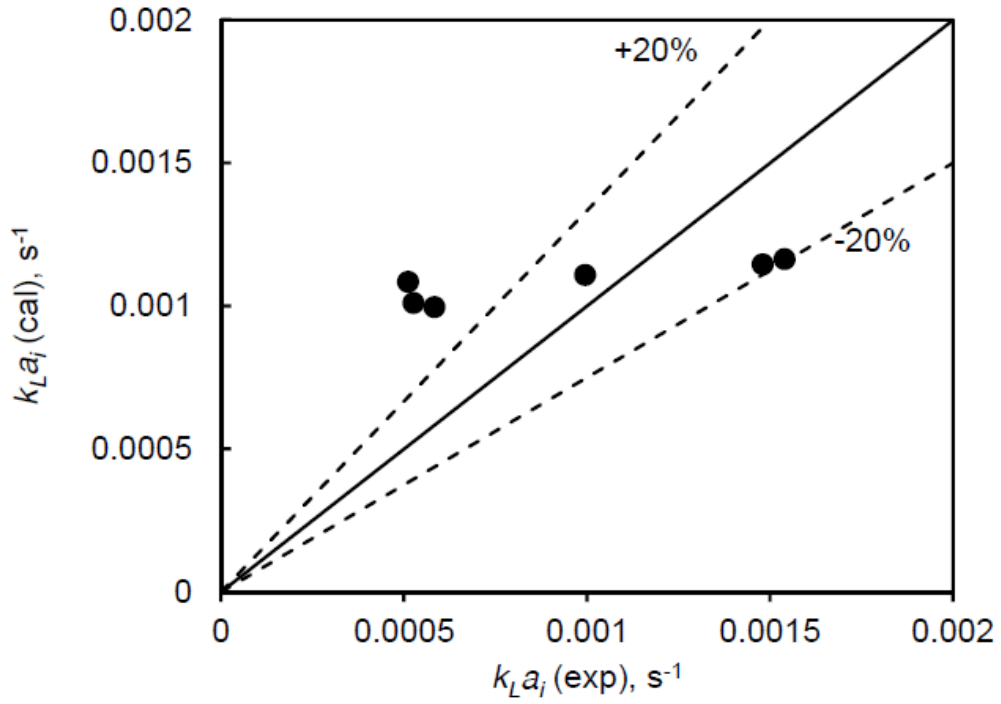

Figure 4.59: Plot of $k_L a_i$ (cal)vs . $k_L a_i$ (exp)

Conclusion of the findings in this work is presented in the next chapter.